Biochemical Engineering Journal 215 (2025) 109623

Contents lists available at ScienceDirect

Biochemical Engineering Journal

journal homepage: www.elsevier.com/locate/bej

Regular article

Flow-following sensor technology, a route to validated CFD models

Cees Haringa [a,*,1], Tannaz Tajsoleiman [b,1], Wouter A. van Winden [c], Daniel Dong [d], Ray M. Gladue [e], Liang Wu [c], Tue Rasmussen [b], Henk J. Noorman [a,c]

[a] Deptartment of Biotechnology, Delft University of Technology, van der Maasweg 9, Delft 2629HZ, the Netherlands
[b] Freesense ApS, Copenhagen, Denmark
[c] dsm-firmenich Science & Research, Delft Biotech Campus, Alexander Fleminglaan 1, Delft 2613 AX, the Netherlands
[d] dsm-firmenich Science & Research, 6480 Dobbin Road, Columbia, MD 21045, USA
[e] dsm-firmenich Asset Technology, 6480 Dobbin Road, Columbia, MD 21045, USA

ARTICLE INFO

Keywords:
Bubble column
Computational fluid dynamics
Flow-following sensors
Pilot-scale
Bioreactor

ABSTRACT

Flow-following sensor technology offers a method to collect information on flow patterns and local velocities in pilot- and industrial scale reactors, which are practically inaccessible to many measurement techniques. Such data is highly valuable for scale-up of bioprocesses, as well as validation of bioreactor CFD simulations. Flow-following sensors were applied in a pilot-scale (2 m^3 filled volume) bubble column fermentor, showing that axially resolved data can be acquired under heterogeneous bubbly flow conditions with high gas holdup. Next the use of the collected data for validation of CFD simulations of the pilot-scale reactor is explored, discriminating between models utilizing different interphase interaction models. The CFD simulation was found capable of capturing the velocity profile and circulation behavior, but full validation was found to be challenging. When simulating virtual sensors via Lagrangian particle tracking, differences are observed in terms of particle distribution and sensitivity to particle density between experimental and simulated data, indicating further development of representative CFD simulations is required.

1. Introduction

The need for non-fossil feedstocks leads to an increasing interest in bioprocesses and biorefineries for bulk applications. While bioprocesses successfully compete with some fossil counterparts, such as the production of selected organic acids and alcohols (especially ethanol), intensification of bioprocesses is instrumental to meet the market demands for many others. Intensification opportunities certainly exist, both regarding micro-organisms (genetic engineering) and process innovation, but the limitations imposed by working with living catalysts does result in industrial bioprocessing largely relying on the workhorses used since its inception: large-volume stirred tanks, airlift-loop reactors and bubble columns [1]. Intensification at the reactor level mainly aims at continuous improvements of these reactor types, relieving transfer limitations and improving spatial homogeneity to avoid undesired responses of the micro-organisms, which may lead to scale-up production losses in the range of tens of percents [2].

Identification and alleviation of the above limitations requires hydrodynamic insights beyond standard engineering correlations, and hence bioprocess engineers increasingly use Computational Fluid Dynamics (CFD) to gain more insight in large-scale multiphase hydrodynamic behavior. However, these models rely heavily on closure relations for turbulence and interphase exchange of mass and momentum. Industrial fermentations - turbulent, strongly aerated, surfactant-laden, and not seldom of non-Newtonian rheology [3,4] - are highly challenging to simulate. This is due to the inherent complexity of the interactions and lack of suitable closure relations for these specific conditions, which leads to the available relations for air-water systems being used beyond their range of (guaranteed) validity. A lack of detailed hydrodynamic data for industrial scale bioreactors hampers validation of current and development of improved CFD approaches. Current validation relies on global quantities (gas holdup, mixing time) and point measurements of e.g. dissolved oxygen, or on comparison with lab/pilot scale data from literature for, as far as available, geometrically similar equipment. For some applications, this approach suffices. Using air-water models, good agreement in mixing time and gas holdup were

* Corresponding author.
E-mail address: c.haringa@tudelft.nl (C. Haringa).
[1] Authors contributed equally.

https://doi.org/10.1016/j.bej.2024.109623
Received 19 July 2024; Received in revised form 3 December 2024; Accepted 26 December 2024
Available online 28 December 2024

observed for a stirred 22 m^3 yeast fermentation [5,6]. Similar approaches were used to validate CFD for pilot-scale reactors [7,8]. Other studies, focused on inclusion of cellular dynamics, omitted complexities such as rheology and accepted course hydrodynamic agreement [2]. Such simplifications are admissible when commenting on *grosso modo* reactor performance with behavior sufficiently close to air-water, but not when investigating finer details for process intensification. Here, consideration of flow-influencing geometric details at full scale [7] and compositional and rheological complexities of fermentation broths [9] is essential.

Neutrally buoyant sensors that follow the internal flow, and register their behavior and surroundings (e.g. acceleration, pressure, temperature, pH, dissolved oxygen concentration (DO)) over time, can provide insights in case-specific local hydrodynamics/conditions [10,11]. Such data can be used to directly troubleshoot fermentations (e.g., identification of stagnant zones or poor mixing, quantification of pH and dissolved oxygen gradients), or for CFD validation at the relevant scale, providing more reliable simulations to scrutinize potential process improvements in-silico. Consequently, several groups have devoted attention to developing and studying flow-following sensors; for a historical overview we refer to Bisgaard et al. [10]. Despite their attractiveness, there are several challenges regarding the application of flow following sensors:

- Their typically centimeter-range size means they have particle response times of O(s), leading to high Stokes numbers in relation to turbulent flow fluctuations [10,12]. As such, sensors may follow the *average* flow in Large reactors (>10 s circulation time) well, but do not capture turbulent variations or fast accelerations accurately. When use for CFD validation, this means direct comparison between sensor data and velocity fields or tracer mixing times may be flawed.
- In aerated systems, the sensor needs to be neutrally buoyant with respect to the average mixture (gas + liquid) density. However, this density may change locally, due to axial and radial gradients in the average gas holdup, as well gas plume oscillations. This is especially true in heterogeneous bubbly flows [13–15].
- Current technology does not allow to quantify the full position of the sensor in the reactor; typically, the registered pressure is used as a proxy for axial position. This does require assumptions on the (local) gas holdup to correlate height with pressure, which may affect the accuracy of the measurement [10].

Recent work by Hoffman et al. in a 15 kL stirred reactor highlights the potential of flow-following sensors, observing compartmentalization inside the reactor, and circulation times in the same range of the global mixing time; in terms of macroscale circulation, the sensors performed appropriately [16].

Comparison between CFD and sensor particle data yielded promising results in stirred single-phase flow [11]. Good agreement was observed with fluid velocities from CFD simulations in quiescent regions, while large offsets are noted near the impeller due to the response time of the sensors [10]. Reinecke et al. similarly note good performance in viscous glycerol, but observe an offset in circulation behavior compared to a liquid tracer in water. Still, good overall circulation behavior was observed [17]. One solution to account for the response time in CFD validation, is to include particles with equal characteristics to the sensors in the CFD simulations, and validate the resulting Lagrangian CFD data against experiments. This approach requires adequate interphase interaction models to capture response of sensors to fluid accelerations. As an example, Hoffman et al. studied the motion of sub-millimeter particles in stirred vessels both experimentally and numerically [12]. The size of the flow-following sensor particles challenges the typical assumption of point particles in Lagrangian CFD, however, while the spatial resolution of typical industrial scale simulations [18] is insufficient to treat them as resolved objects. As such, further insight in the utilization of Lagrangian particles to represent flow-following sensors in CFD simulations is required.

A limited number of studies has applied flow following sensors in aerated systems, but the acquired data has not been used for comparison with CFD simulations. The studies did observe good macro-scale circulation behavior, despite the abovementioned challenges [17,19], even if the sensor density was not exactly matched to the mean mixture density; Reinecke et al. did observe an offset in positional distributions for a 2 % mismatch in density, but required a 6 % density difference for full flotation of the sensor [20], which implies using sensors with different densities can be used to comment on the global gas holdup, but also that sensors with some density offset can be used for CFD validation, provided Lagrangian CFD with equal particle characteristics is employed. However, the flotation experiments of Reinecke were conducted in a stirred, single-phase liquid; industrial-scale pneumatic bioreactors often operate with high superficial gas velocity (> 0.05 m/s), leading to highly dynamic heterogeneous flow, which is more challenging to model, and which may impact the behavior of flow-following sensors due to gradients in gas holdup (and therefore apparent fluid density) [14,15].

In this study, we analyze the application of *"FermSense 3D"* sensor technology in a vigorously aerated system. Our main hypothesis is that, despite experimental challenges, flow following sensors can provide data on local hydrodynamics that can be used for the verification of CFD models. To evaluate this, we conducted an experimental study in a pilot-scale (2 m^3 liquid volume) bubble column, operated by the DSM-Firmenich. We exhibit what data can be acquired with flow-following sensors and compare experimental data with Euler-Lagrange ('sensor point of view') CFD simulations, and discuss applicability of the approach as well as limitations and challenges regarding the application of mobile sensors and associated CFD simulations in high gas velocity bioprocesses. The focus therein is to assess whether and how we can use sensor data to discriminate between the performance of several CFD models with different assumptions related to interphase exchange models in simulating fluid behavior in the pilot-scale bubble column; further adjustment of the assumptions to improve the match between simulation and experiment is out of the current scope.

2. Materials and methods

2.1. Freesense "FermSense 3D" technology (incl. data processing)

The general principle of Lagrangian measurements, using mobile 'sensors', has been around for decades. A range of macroscopic tracer particles [12], radio- and magnetic pills ([21–23]) and radioactive particles (e.g. [24,25]) have been used to study the fluid flows and circulation patterns. These methods rely on external detectors, however, which is typically incompatible with industrial equipment. This has led to the development of wireless sensor particles with a built-in positioning system which can be applied in large-scale reactors; for a comprehensive review of wireless sensor technology, we refer to [10].

Fig. 1. *FermSense 3D* sensor.

FermSense 3D (Fig. 1) is a flow-following sensor device particularly designed for spatial measurements inside pilot to industrial scale bioreactors [11]. The device is equipped with pH or dissolved oxygen, pressure, temperature and accelerometer sensors with sampling rate up to 5 Hz. The sensors and the electronics are encapsulated in 32–55 mm spherical shell made of polyether ether ketone (PEEK). The device is designed to resist high-temperature sterilization, chemical cleaning procedures, pressurized conditions and collision impacts from the impeller and other solid internals in the bioreactor. Since the sensor is substantially larger than the mean bubble size, the density of the sensor is adjusted to match the average apparent density of the gas-liquid mixture to achieve neutral buoyancy [10,26], by addition of internal weights. The axial position y and velocity v_y of the sensor device are determined using the pressure measurements [11].

2.2. Pilot-scale operating conditions

Experiments were conducted in a pilot scale bubble column with a working volume of 3.3 m^3.The dimensions are listed in Fig. 2. Air is sparged via three pipe spargers in a triangular orientation, at an off-bottom clearance of approx. 0.23 m; the airflow is controlled using a Coriolis mass flow meter calibrated to normal condition at 1 atm and 25 deg. C. We selected a superficial gas velocity Table 1 reports the operating conditions that were used for the trial reported in this work. The overall gas holdup was measured using an ABB/K-Tek LLT100 Laser level transmitter with a range of 2–330 feet providing continuous level measurement. It's mounted on a 4'' diameter sight glass. The mixing time was quantified through the addition of a small amount of $MgSO_4$ solution at vessel top, and offline quantification of the magnesium concentration using ICP, in samples acquired every 5 seconds at an axial position $h_{samp} = 0.23m$. However, this was done under operating conditions somewhat deviating from this study; hence the mixing study only serves for qualitative comparison.

2.3. FermSense application

Five *FermSense* devices with a diameter of 52 mm were inserted in the reactor, measuring pressure, pH and temperature with a frequency of 5 Hz. The average gas-liquid mixture density was conducted based on a-priori estimation of the column gas holdup using two literature correlations. The correlation of Heijnen and Van 't Riet [27], $\overline{\alpha_g} = 0.6\, v_s^{0.7}$, was based on global gas holdup measurements in experiments prior to 1984, but shows agreement with some contemporary studies [28]. Here, v_s is the pressure-corrected superficial gas velocity. The correlation of Maximiano Raimundo et al., $\overline{\alpha_g} = 0.49\, v_s^{0.41} \cdot D_R^{-0.047}$, was based on more recent experiments including local gas-holdup profiles [14,15]. While not stated in the paper, communication with the author indicates that v_s is based on Q_g at STP, which omits the effect of gauge pressure. To avoid over-estimation of the holdup, the pressure-corrected v_s is currently used instead. The estimated gas holdup using both models is added in Table 1. There is a substantial disagreement between the two correlations, which may be due to differences in sparger geometry and water quality, something that deserves further scrutiny but is outside of the current scope. To cover the density range indicated by the a-priori estimations, it was decided to apply devices with three different densities: 0.77 kg/L, 0.87 kg/L and 0.90 kg/L, matching 23, 13 and 10 % global gas holdup, respectively.

With the current state-of-the-art, the 3D trajectories of the devices cannot be directly reconstructed from the accelerometer data, and spatial information is limited to the axial position and velocity, based on pressure sensor data. Use of the accelerometer data for further insight remains a topic of future investigation. The axial position is based on the hydrodynamic information available from the pressure sensor and derived using the pascal's law $P_{meas} = P_{ref} + \rho_f g \Delta h$, with Δh the distance from the reference location, and ρ_f as fluid apparent density. We assume a constant ρ_f in this case, omitting the notion that ρ_f may be a function of axial position due to expansion of the gas [10,29]. We expect this effect to be minor, and also observe no strong dependency of gas holdup on axial position in our CFD simulations (including variable bubble size and gas density). Our CFD simulations furthermore showed no radial variation in total pressure resulting the radial gradient in (average) holdup, which is in line with the assumptions made when using differential pressure measurements for overall holdup determination. Besides the above assumption, the accuracy of height measurements may be affected by local pressure fluctuations ($\sigma_P \approx$ 30 Pa at the set conditions [13], translating to 3 cm), sensor resolution (0.39 Pa) and response time (~10 ms, translating to 1 cm displacement at 1 m/s velocity).

The axial velocity is calculated from the time derivative of position [11,30], assuming a constant velocity in the time between two measurements (0.2 s), justified by a particle response time $\tau_p > 1$ second [10]. The circulation time distribution was determined by registering time intervals between consecutive passages through detection planes at fixed heights [11]; four planes were set up, starting at 1 m from the bottom, with a mutual clearance of 1 m.

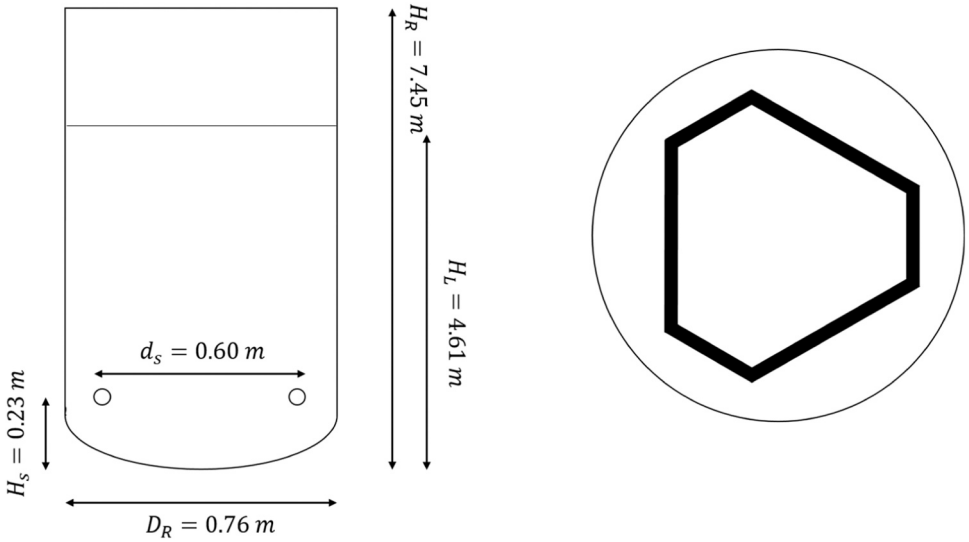

Fig. 2. Illustration of the bubble column (not to scale). Right: top-down view of the sparger geometry. In reality, the sparger consists of three pipes with a single bend; these have been connected in the current model to avoid the meshing complexities of blunt ends.

Table 1
overview of conditions applied and expected in this study. The estimated gas holdup based on the correlations of Heijnen and van 't Riet [27], and Maximiano Raimundo [14] have been added for the a-priori estimation of the apparent density, given in the last column.

Liquid mass (kg)	Q_g (l/min)	P_g (kPa)	v_{sg} at mean P (m/s)	$\overline{\alpha_g}$(%) Van't Riet	$\overline{\alpha_g}$ (%) M. Raimundo	ρ_{eff} (kg/L) Van't Riet	ρ_{eff} (kg/L) M. Raimundo
2100	5000	27.6	0.121	13.7	20.9	0.863	0.790

The following metrics can be used to compare the data of experimental devices with that of virtual particles in CFD simulations [11]:

- Probability distribution of particle presence as a function of reactor height.
- Probability distribution of particle axial velocity as a function of reactor height.
- Circulation time distribution of particles in the reactor.

2.4. CFD simulations

2.4.1. CFD modelling of heterogeneous bubble columns

CFD simulations of heterogeneous bubbly flow are challenging, due to the presence of bubble coalescence and breakup and swarm effects in the system, and the wide range of interphase closure models available. While it is not our aim to provide a comprehensive review, we discuss some key aspects to support our modelling choices and facilitate later discussion.

2.4.1.1. Interphase interaction models. Most studies engaging in bubble column focus on the homogeneous flow regime, where well validated models are available [31,32]. The broad size distribution and prominent bubble size dynamics, and non-linear relation between bubble size and interphase forces, make modelling of heterogeneous flow highly challenging and, especially in case bubble size dynamics are included, computationally demanding [33]. Still, promising results are reported in literature for air-water systems [34–38], which is the current scope. The selection of interphase interaction models is key in setting up bubble column simulations. Comprehensive reviews are available [39–42], here we summarize key takeaways that informed our model selection. The drag force is the most important interphase force, but while a plethora of models is available, most models produce similar and accurate bubble drag coefficients, provided they distinguish between shape regimes [43,44], and as such the specific drag model will have limited impact. The effective drag in highly aerated flows is strongly reduced due to swarm effects, originating from bubble wakes [45]. The exact impact of this is ill-understood, and seems to depend on size distribution [46]. McClure et al. also noted a dependency on sparger type, with an earlier onset and more pronounced effect when using spargers that introduce heterogeneous flow even at low superficial gas velocity [47]. The lift force is a pseudoforce describing lateral motion of bubbles due to velocity gradients; this force is relevant in heterogeneous flow columns as its magnitude depends on bubble diameter, and the direction of motion switches direction from outward to inward around a bubble diameter of 5–6 mm [48]. While this can lead to size segregation that in turn can affect the holdup profile, the notion that the direction change lies close to the typical mean bubble diameter in heterogeneous bubble columns leads to limited impact [49]. The virtual mass force is only active in regions of high acceleration and similarly has limited impact [39,50]. Opinions on inclusion of turbulent dispersion, a pseudo-force that accounts for local bubble redistribution due to turbulence, are mixed. Some authors observe better agreement with the parabolic flow profile in heterogeneous bubble columns [39] while others report 'flattening' of flow profiles [51]. McClure et al. did include turbulent dispersion in their models, but did not explicitly assess its impact [49].

2.4.1.2. Turbulence modelling. There is relatively little explicit attention to turbulence modelling for bubble columns. Most studies use a variant of the k-epsilon approach, with some favorably commenting on the RNG model [52,53]. Several studies note the importance of including bubble induced turbulence (BIT) [34,53,54]. In our own preliminary simulations (using [36] for validation) we observed highly similar behavior between RNG and realizable k-epsilon for liquid velocity and holdup, with the realizable model yielding somewhat better agreement on turbulent kinetic energy. The inclusion of BIT had limited impact on velocity profiles, but proved essential for the prediction of the global energy dissipation; an essential aspect in case a bubble population balance model is included to predict the size distribution.

2.4.1.3. Bubble size modelling. Although bubble sizes are broadly distributed in heterogeneous bubble columns, the high computational costs of population balance models means often simplified models are used [34], [49,53,55]. Two-class models such as the Energy Minimization Multiphase Multi-Scale model (EMMS) have also shown promising results [56], but this approach is not readily available in the utilized CFD software. Population balance approaches have been used to predict bubble size distributions [46,57–59], albeit at substantial computational cost [33]. A dynamic single-bubble size model offers an attractive alternative in terms of computation time, although such models are not natively available in the used software [33].

Experimentally, the average bubble size in heterogeneous flow bubble columns was determined to be around 6–8 mm [3,14]; we do not have data on the bubble size in the column currently under investigation.

2.4.2. Selection of approaches

Based on this review of literature, we concluded the following for our approach:

- The specific drag model and k-epsilon variant is of limited impact.
- Lift and virtual mass are excluded based on their limited impact.
- Drag modification (swarm effects) are essential and pronounced due to the heterogeneous sparger installed in the used column.
- Lacking an a-priori bubble size measurement, a bubble size model is preferred.

We conducted a number of preliminary simulations comparing results with the $v_s = 0.12 m/s$ data presented by Sanyal et al. [36], being similar to the conditions studied in this work. Based on this, the realizable turbulence model with the Troshko-Hassan BIT model was selected as the baseline approach. The mixture turbulence formulation was selected, as the dispersed model exhibited stability issues when using higher order discretization schemes, which was observed to be necessary to avoid overtly flat profiles [53]. We applied QUICK discretization for all equations. Turbulent dispersion was equally excluded; during the preliminary simulations we observed either unrealistically flat holdup profiles, or struggled with numerical stability.

In our first round of simulations, four cases were defined. Herein, we varied (1) drag reduction model/magnitude and (2) bubble size model/mean diameter.

Case A. The universal drag model is used, based on strong prior performance in stirred tanks [5]. Due to the built-in Richardson-Zaki drag reduction model underpredicting drag modification [49], a high gas holdup is expected. A constant bubble diameter of 7.5 mm was used

[14].

Case B. The Tomiyama drag model was used, with a deliberately high bubble diameter (13 mm) and a strong, constant swarm modification factor ($C_D = 0.12\,C_{D,0}$). This is expected to lead to a low global gas holdup. In this case we additionally made changes to the turbulence setup; the dispersed formulation was used, following Fletcher et al. [34]; to facilitate numerical stability, discretization of the turbulence equations was changed to 1st order, and BIT was omitted. Unpublished testing results show these changes have a large impact on overall energy dissipation, but not on velocity and holdup in case of a fixed bubble size.

Case C. The Tomiyama drag model was used, with the McClure drag modification, for coarse sparger columns [47]. A population balance model was used to predict the bubble size distribution. This setup is expected to lead to moderate gas holdups.

Case D. As above, but a constant swarm modification of moderate strength ($C_D = 0.175\,C_{D,0}$) was used, following observed issues with Case C.

The specific setups deliberately selected to yield a low, moderate and high gas holdup, to study the possibility to discriminate between models based on the experimental device data, rather than as a structured study towards the impact of particular sub-models. It was our aim to subsequently explore further modelling options (e.g. further variations in bubble diameter, drag modification and turbulence setup) but this was not pursued following consistent offsets between computational particle motion and experimental data. A complete overview of model settings for the four cases is provided in Table 2.The CFD simulations were conducted in ANSYS FLUENT 2020R1. A mesh of 215k polyhedral elements, with local refinement near the sparger, was used. In all cases, the CFD simulations were time resolved with $\Delta t = 0.005$.

2.4.3. Bubble size modeling

As indicated above, a fixed bubble size is used in Cases A and B. Cases C and D use a discrete population balance approach to predict rather than prescribe the bubble size, with 13 bins and a size range from 0.5 to 12.8 mm. The homogeneous population balance model is employed, meaning that a single flow field is used for the dispersed phase, and interphase forces are computed based on the local Sauter mean bubble diameter. The Luo & Svendsen coalescence and breakup model were adopted.

2.4.4. Interphase exchange models: gas-liquid flow

2.4.4.1. Drag force. A drag model is required to compute the drag coefficient of individual bubbles of different sizes and shapes. In high-velocity heterogeneous gas flow, the drag force acting on individual bubbles is substantially affected by swarm effects, particularly drag reduction due to wake effects. Case A uses an interphase closure approach based on a fixed bubble size and the Universal drag model (Eq. 1), based on the Ishii-Zuber drag model [60], following successful application in prior aerated stirred-tank studies [2,5,6].

$$C_{D,vis} = \frac{24}{\mathrm{Re}}\left(1+0.75Re^{0.75}\right), \quad C_{D,dis} = \frac{2}{3}\left(\frac{d_p}{\lambda_{RT}}\right)\left(\frac{1+17.67\ f^{\frac{6}{7}}}{18.67f}\right)^2, \quad C_{D,cap} = \frac{8}{3}(1-\alpha_g)^2 \tag{1}$$

Where $f = (1-\alpha_g)^{1.5}$, $\lambda_{RT} = \sqrt{\frac{\sigma}{g\Delta\rho}}$ and $Re\left(\frac{\rho_l d_b u_b}{\mu_l}\right)$ the bubble Reynolds number. The drag coefficient $C_{D,bub} = \max(C_{D,vis}, \min(C_{D,dis}, C_{D,cap}))$. In the universal drag model swarm effects incorporated through the $(1-\alpha_g)^m$ term, with m = 1.5 or 2 depending on the regime.

In Cases B-D, the Tomiyama model [43] for contaminated water is used to compute the drag coefficient, Eq. 2:

$$C_{D,bub} = \max\left(\min\left(\frac{24}{\mathrm{Re}}\left(1+0.15Re^{0.687}\right), \frac{72}{\mathrm{Re}}\right), \frac{8}{3}\frac{Eo}{Eo+4}\right) \tag{2}$$

Here, Eo is the Eotvos number $\left(\frac{\Delta\rho g d_b^2}{\sigma}\right)$. The Tomiyama model does not contain a swarm correction, meaning that for Cases B-D an additional swarm correction model is required, with $C_{D,swarm} = f(\alpha_g)C_{d,bub}$. Swarm drag models have been devised by Simonnet et al. [45], which includes the homogeneous-heterogeneous transition, and McClure et al. [47], who noted that $f(\alpha_g)$ depends on the sparger type, and that for typical industrial spargers, flow is heterogeneous even at low v_s. Under such conditions, f was found to be approximately constant in their work (albeit with much scatter). In the current study, the 3-tube sparger with a coarse hole configuration is expected to provide heterogeneous flow under all conditions. In Cases B, a constant value of $f(\alpha_g) = 0.12$ was applied as a scenario with strong swarm effects. In Case C, the volume-fraction dependent swarm modification model of McClure et al., Eq. 3, with $n = 50$ and $b = 0.08$ was used [47].

$$f(\alpha_g) = \min\left((1-\alpha_g)^n + b, 1\right), C_D = f(\alpha_g)C_{D,bub} \tag{3}$$

As we observed unrealistic plume behavior using this model, a constant value $f(\alpha_g) = 0.175$ was again adopted for Case D.

2.4.4.2. Bubble-induced turbulence (BIT). Bubble induced turbulence (BIT) was included in all simulations except Case B using the Troshko-Hassan formulation [61], Eq. (4);

$$\Pi_{k,m} = C_{ke}K_{gl}\left|U_g - U_l\right|^2, \quad \Pi_{\epsilon,m} = C_{td}\ \frac{1}{\tau_{BIT}}\Pi_k \tag{4}$$

Where $\tau_{BIT} = \frac{2C_{VM}d_p}{3C_D\left|U_g-U_l\right|}$ is the bubble induced turbulence timescale, and $K_{gl} = \frac{\rho_g d_p}{6\tau_p}\frac{C_D\mathrm{Re}}{24}A_i$ the interphase exchange coefficient, with A_i the interfacial area concentration and $\tau_p = \frac{\rho_g d_p^2}{18\mu_l}$ the particle relaxation time.

2.4.5. Particle tracking

To emulate the motion of the *FermSense* sensors, the discrete phase model of FLUENT was utilized, which represents discrete entities as inertial point particles. Considering the size of the sensor devices, this is a major assumption, but computationally, resolved particle models are not feasible with the resources used in this study. As in the experimental run, particles of different densities (0.77 kg/L, 0.87 kg/L and 0.90 kg/L) were released in the simulation. Since tracking particles for hours in the CFD simulations is impractical, 250 particles of each density were

Table 2
CFD modeling settings used in this study. 1st o. upw. stands for 1st order upwind discretization.

Case	A	B	C	D
Drag model	Universal drag	Tomiyama	Tomiyama	Tomiyama
Swarm modification	$(1-\alpha_g)^m$	0.12 (fixed)	McClure	0.175 (fixed)
BIT	Troshko-Hassan	None	Troshko-Hassan	Troshko-Hassan
Bubble size	7.5 mm (fixed)	13 mm (fixed)	Pop. Balance, Luo & Svendsen	Pop. Balance, Luo & Svendsen
Gas density	Ideal gas	Ideal gas	Ideal gas	Ideal gas
Turbulence	Mixture	Dispersed	Mixture	Mixture
Discretization	QUICK	QUICK (momentum) 1st o. upw. (turbulence)	QUICK	QUICK

tracked for a few minutes to collect motion statistics, relying on ergodicity for comparison. These inert particles respond to motion of the mixture phase (gas and liquid). Turbulence was imposed via the discrete random walk model [62]. The acceleration of the inert particles is computed from the particle momentum balance, Eq. 5:

$$\frac{m_p dU_p}{dt} = \frac{m_p(U_f - U_p)}{\tau_p} + \frac{m_p(\rho_p - \rho_f)}{\rho_p} + F \tag{5}$$

Where τ_p is the particle relaxation time, and F represents forces other than buoyancy and drag; the relevant forces are selected by the user, and are mainly dependent on the particle scale and density ratio to the surrounding. In the current study, the virtual mass force and pressure gradient force were included, Eq. (6):

$$F_{VM} = C_{VM} m_p \frac{\rho_l}{\rho_p}\left(U_p \nabla U_f - \frac{dU_p}{dt}\right) \quad , \quad F_{PG} = m_p \frac{\rho_l}{\rho_p} U_f \nabla U_f \tag{6}$$

These forces are relevant when the discrete and continuous phase density are close (the Fluent manual recommends inclusion $\frac{\rho_l}{\rho_p} > 0.1$). Other forces, related to rotation of the particle, were currently omitted. The drag coefficient was based on the spherical drag law of Morsi and Alexander [63], not accounting for rotation of the particles.

2.4.6. Solution procedure

The gas-liquid hydrodynamics are solved in transient mode for approx. 100 seconds until the flow field has stabilized. The timestep size is varied during this period, starting with coarse steps to quickly establish the rough flow field, and then refining the step size for accuracy. Eventually, a step size of $\Delta t = 0.005s$ was used. Besides the discretization schemes listed in Table 2 the PRESTO! Scheme for pressure discretization, and SIMPLE for P-V coupling. Once the flow field was established, the particles were released over the height of the column and mixed for at least 100 seconds to ensure they were fully distributed through the domain, as to avoid positional bias in the tracking results. Then, particles were tracked for at least 88 seconds, logging the position, velocity of the particle, velocity of the surrounding liquid, and pressure along the particle trajectory. In order to compare the gas holdup profiles with literature sources, flow variables have additionally been averaged over the time period.

2.4.7. Liquid phase mixing study

Liquid phase mixing was studied for Cases B, C and D using an Eulerian tracer. After establishing the flow field, a spherical region (radius 0.08 m) at a position just below the surface is patched with a tracer concentration of 1. For Cases B, C the location is $[r, y, \theta] = [0.141m,\ 4.6m,\ 45^o]$, for Case D $[r, y, \theta] = [0.141m,\ 5.1m,\ 45^o]$, following the higher holdup. The tracer diffusivity was set at $\mathscr{D} = 6{\cdot}10^{-10}\frac{m^2}{s}$, other properties were equal to water. The simulation was continued with $\Delta t = 0.005s$ until mixing was complete for Cases B and D, and for ca. 250 s in case of C. Mixing was studied by registering the tracer concentration as a function of time at 12 positions, with $r = 0.1$, 0.3 m, $y = 0.5,\ 2.5,\ 4.5$ m and $\theta = 0,\ 180^o$. The 95 % mixing time was quantified in two ways; first, by registering the last timepoint for which the dimensionless concentration $\frac{C_s}{\overline{C_s}} < 0.95$ or $\frac{C_s}{\overline{C_s}} > 1.05$, and second, by computing the coefficient of variation [64], Eq. 7:

$$CoV = \sqrt{\frac{1}{N_{pt}}\Sigma_i\left(\frac{(C_i - \overline{C_s})}{\overline{C_s}}\right)} \tag{7}$$

Since the CoV is based on a number of point-probes in this case, no volume weighing is applied (in contrast to Hartmann et al., who base the CoV on all control volumes, [65]). We do adhere to the threshold of Hartmann et al., $CoV = 0.0283$ for 95 % mixing.

2.5. Device velocity estimation in a radial density gradient

The mobile sensor device density is tuned to the average effective mixture density, ρ_{eff}. In reality, the gas holdup will not just be dynamic, but will also feature consistent axial variation (due to the static pressure gradient) and radial variation (due to plume formation) in the local average mixture density. This means the sensor device will not be *locally* neutrally buoyant, which may impact the apparent overall neutral buoyancy, and lead to differences in expected and observed settling behavior for a device with a given density as a function of gas holdup. A reduced settling velocity was observed by van Barneveld et al. [66], using a 3 cm radio pill with a density equal to water. They attributed the reduced settling velocity to adherence of bubbles to the sensor, increasing its buoyancy. However, the observed effect (~30 % reduction in v_{term}) appears too strong for this explanation; an over 10 % apparent density reduction is required to match the observed behavior at high holdup. Hence, we explore whether the radial variation in gas holdup in heterogeneous bubbly flow may impact the apparent neutral buoyancy. An estimation of the impact of the radial holdup gradient [14,36] on sensor motion was made, estimating the local terminal velocity of the sensor with respect to the liquid as a function of radial position, resulting from the mismatch in device density ρ_p and the local average mixture density $\rho_{mix}(r)$. This was done through a terminal velocity model implemented in MATLAB. The model assumes that a device instantly adapts to the terminal velocity v_{term} (a major assumption, given the Stokes number [10,12]). v_{term} is governed by the balance between drag and buoyancy, Eq. 8.

$$v_{term}(r) = \sqrt{\frac{4gd_p}{3C_D}\left(\frac{\rho_p - \rho_{mix}(r)}{\rho_{mix}(r)}\right)} \tag{8}$$

For simplicity, turbulent flow around the sphere was assumed, giving $C_D = 0.44$. This introduces some error when ρ_p is close to the mixture density, but is appropriate at most positions as $Re_p > 1,000$, and avoids iterative solution. Here, $\rho_{mix}(r)$ is the local average mixture density as a function of radial position, calculated as $\rho_{mix}(r) = \alpha(r)\rho_g + (1 - \alpha(r))\rho_l$. Maximiano Raimundo et al. [14] give a correlation for the radial gas holdup $\alpha(r)$, Eq. 9:

$$\alpha_g(r) = \overline{\alpha_g}\cdot\left[-1.638\left(r^6 - 1\right) + 1.228\left(r^4 - 1\right) - 0.939\left(x^2 - 1\right)\right] \tag{9}$$

With $\overline{\alpha_g}$ the overall gas holdup of the reactor. The profile in Eq. 9 can be used to calculate the radial mixture density profile, and substituted into Eq. 9 to compute the terminal velocity as a function of radial position. The particle velocity then follows from $v_{part} = v_{liq} - v_{term}$, with Eq. 10 describing radial profile in liquid velocity v_{liq} [14]:

$$v_{liq}(r) = \frac{v_0}{1.128}\left(2.976\exp\left(-0.943 \quad r^2\right) - 1.848\right), \quad v_0 = 1.35 \quad v_s{\cdot}D_R^{0.4} \tag{10}$$

The average particle axial velocity is calculated by area-weighted averaging of the velocity profile, Eq. 11:

$$< v_{part} > \quad = \frac{\int v_{part}(r){\cdot}2\pi r dr}{\int 2\pi r dr} \tag{11}$$

With this, we can judge if a device behaves as neutrally buoyant for a given mean gas holdup, in which case $< v_{part} > \quad = 0$. When $< v_{part} >$ is above 0, the device will show net. upward motion at a given gas holdup, indicating radial mixture density variations reduce settling, while a negative $< v_{part} >$ signals enhanced settling.

3. Results and discussion

In this section, we will first analyze the experimental data acquired with the mobile sensor devices, followed by the CFD study. The section closes with a comparison between the experimental data and the CFD

simulation.

3.1. Experimental assessment: device buoyancy and gas holdup

First, we consider the motion registered by the sensor device. Fig. 3 shows an example of the axial movement of 3 sensor devices (0.77 kg/L, 0.87 kg/L and 0.9 kg/L densities) in the tested bubble column. The dominant movement of the lightest device at the upper part of the liquid indicates lower density of the sensor compared to the fluid apparent density, leading to the device mostly circulating in the column top. In comparison, the other two devices showed more uniformly distributed movement through the liquid, which indicates that density of these two sensors is closer to the fluid apparent density under the tested condition. Based on the device apparent density, this translates to a gas holdup in the range 10–13 %, consistent with the estimation by the Van 't Riet correlation (13.7 %), and much lower than the correlation and measurements of Maximiano Raimundo (20.9 %, based on the pressure-corrected v_s). However, measurements with the stationary level sensor were done in an earlier run under similar conditions and indicated a gas holdup of 21.5 %, which is consistent with the correlation of Maximiano Raimundo et al., and substantially higher than indicated by the Van 't Riet correlation and floating device measurements. While these observations appear in conflict, they are in agreement with radio pill experiments by van Barneveld et al. [66] who observed settling velocities that were lower than expected for a given mixture density. An open question is why this change in settling velocity (and consequently, effective neutral buoyancy) occurs. Van Barneveld et al. suggest adherence of air bubbles inducing an additional buoyancy effect. A mechanism where devices preferentially reside in regions of lower holdup and hence higher mixture density could also be imagined. Third, we have to keep in mind that, on average, a radial gradient in holdup and hence mixture density exists; we hypothesize that this gradient would lead to neutrally buoyant behavior at a different gas holdup than the device density was tuned for; the mathematical model presented Section 2.5 was developed to test this hypothesis. The results detailed in Section 3.2 show that the indeed this may have an impact. Still, even considering this effect, there is a discrepancy between the estimation based on neutrally buoyant device measurements and the level sensor, which deserves further scrutiny.

3.2. Modelling the impact of the radial holdup profile on sensor movement

The (radial) holdup profile can result in a difference between the liquid density at which the sensor behaves as neutrally buoyant, and the density for which the device is calibrated. This may contribute to the abovementioned discrepancy between static sensor reading, and device behavior. The terminal velocity model was used to estimate the impact of the radial holdup gradient. The holdup at which the device is neutrally buoyant (criterion: $|<v_{part}>| < 0.001 m/s$) can be computed for a given v_s, which is reported in Table 3 for the tested conditions. The holdup at which the model predicts neutral buoyant behavior is 2–3 % higher than the holdup associated with direct density matching, indicating radial gas holdup gradients are expected to lead to reduced settling behavior. The impact is modest, however, with a relative offset of at most 20 %, not fully explaining the gap between static sensor and device measurements. Additionally, the mean particle velocity for the holdup exactly matching the device density is reported, with a more positive velocity (upward) meaning that the device is exceedingly likely to be found near the fluid surface.

3.3. CFD results

3.3.1. Global assessment of flow behavior

The four interphase closure approaches resulted in vastly different gas holdup and flow behavior; an overview of global quantifications is presented in Table 4. Case A, using the universal drag model, yielded a gas holdup of $\overline{\alpha_g} = 0.33$, whereas the other approaches predict

Table 3
apparent neutral buoyancy of the sensor devices accounting for the radial gas holdup profile. 2nd column: gas holdup when the mixture density exactly matches the sensor density (not accounting for radial variation). 3rd column: holdup required to achieve neutral buoyancy when the superficial gas velocity is fixed to the pressure-corrected superficial gas velocity for the provided operating conditions. 4th column: the mean particle velocity when the holdup is fixed to the values from column 2.

$\rho_p \left(\frac{kg}{m^3}\right)$	Holdup matching ρ_P	Neutral buoyancy, $v_s = 0.121 m/s$	Mean particle velocity at $v_s = 0.121$ m/s and holdup based on ρ_P
770	$\overline{\alpha_g} = 23.0\%$	$\overline{\alpha_g} = 26.3\%$	$<v_{part}> = +0.133 m/s$
870	$\overline{\alpha_g} = 13.0\%$	$\overline{\alpha_g} = 15.4\%$	$<v_{part}> = +0.114 m/s$
900	$\overline{\alpha_g} = 10.0\%$	$\overline{\alpha_g} = 12.1\%$	$<v_{part}> = +0.107 m/s$

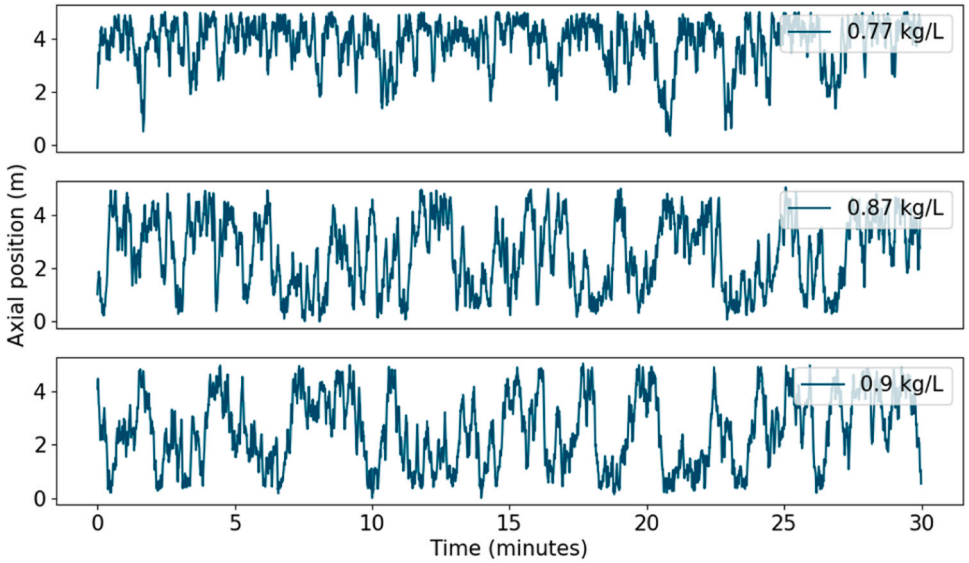

Fig. 3. Registered axial position of mobile sensors with three different densities; the position is derived from the pressure reading by the sensors.

Table 4
gas holdup, observed flow pattern, bubble size and energy dissipation per unit volume for various models. The liquid mass varies slightly between cases due to mass imbalances in the first timesteps, and due to overflow in Case A.

Case	Van 't Riet estimation	M. Raimundo Estimation	A	B	C	D
Gas holdup $\overline{\alpha_g}$ (%)	13.7	20.9	33.0	12.6	13.0	16.4
Flow pattern	Oscillating	Oscillating	Oscillating	Oscillating	Static	Oscillating
Energy diss. (m^2/s^3)	1.32	1.32	1.14	0.4	Nd	1.20
Bubble size (mm)		~7.5	7.5	13	nd	8.7
Liquid mass (kg)	2100	2100	2000	2100	2050	2070

substantially lower values of $\overline{\alpha_g}$, between 0.12 and 0.17. Based on this, Case A can be ruled out: the high gas holdup leads to overflow of the vessel (Fig. 4), also obvious from a reduction in liquid mass compared to the initial 2100 kg. The gas holdup of the other cases is, however, consistent with the range covered by the device and level sensor data. We do note all simulations show some decrease in liquid mass compared to the initialized value, due to small but non-zero liquid fraction in the headspace and poor closure of the mass balances in the first few timesteps. We deem these offsets sufficiently small to be inconsequential for further analysis. Case C exhibits a stable dual-plume structure originating from the sparger, with the only difference between this case and Case D being the volume-fraction dependent drag reduction model. Recent work by Gu et al. with a similarly narrow sparger did not show this issue [67]; the most notable difference in model setup is the lack of turbulent dispersion in our case. Our hypothesis is hence that the narrow sparger leads to a high local holdup, which combined with the aggressive local drag reduction leads to stable 'low drag' channels; turbulent dispersion would work against this as it leads to radial gas distribution based on the hold-up gradient, which would explain why this plume stabilization was not observed by Gu. Additional trials with a single bubble size instead of a population balance, use of the dispersed turbulence formulation (with 1st order turbulence equations), and use of the Simonnet rather than McClure correction model did not affect behavior. Stability issues with turbulent dispersion prevented us from inclusion of turbulent dispersion, and we opted for using a constant swarm factor in Case D instead. Cases B and D both exhibit dynamic behavior, with roughly similar gas holdup, despite different model selections. Cases A and D, which include Bubble Induced Turbulence (BIT), reasonably predict the expected energy dissipation (ε) of 1.32 m^2/s^3 based on thermodynamic considerations [68], while in Case B, where BIT was omitted, ε was strongly underestimated. However, as prior unpublished work conducted on the Sanyal et al. case [36] revealed that the liquid velocity and gas holdup profile (at a given bubble size) were not notably affected by inclusion of BIT, this observation cannot be used to discriminate between Cases B and D in terms of gas holdup and flow behavior; in sections 3.4.2 and 3.4.3 we will explore the potential of the sensor devices in this respect. Of course, proper prediction of ε will be relevant when other models which rely on ε, such as mixing, mass-transfer [69] and breakup kernels in population balances are added, and as such the inclusion of BIT is recommended.

3.3.2. Mixing study

To further compare the predictions of the CFD simulations, a mixing study was conducted for Cases B, C and D, using 12-point monitors throughout the domain (3 axial and 4 radial positions), with a tracer injection at the vessel top. We do note that due to the transient nature of the flow, significant variation in mixing time between repeated simulations and experimental runs may occur [70]. Here, we consider single experiments and simulations, which should hence be interpreted as a ballpark estimation. Fig. 5 shows the tracer response curves for the three cases. While Cases B and D again show qualitatively similar behavior, mixing in Case C is distinctly slower: the simulation was stopped after 250 s, with τ_{95} not yet achieved. The mixing correlation by Groen et al. [71] assuming heterogeneous flow in a bubble column, $\tau_{95} = 1.6 \frac{T^{\frac{2}{3}}}{(gv_s)^{\frac{1}{3}}} \left(\frac{H_L}{T}\right)^2$, predicts a mixing time of 46.0 – 56.7 s depending on the liquid height; for Case D good agreement is observed (Table 5). For Case B, mixing is notably faster than expected. The underlying reason seems to relate to the under-estimation of ε, which in turn leads to a higher value for the turbulent viscosity μ_t and consequently turbulent diffusivity $\mathscr{D}_t$. This observation highlights the importance of including BIT and proper estimation of energy dissipation.

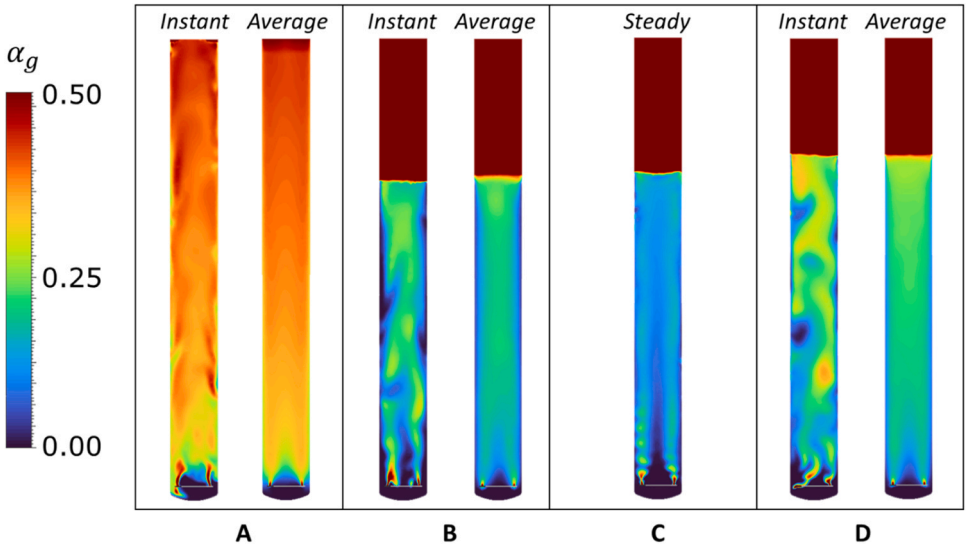

Fig. 4. Predicted gas holdup in the bubble column for the various CFD models, instantaneous and time-averaged. For Case C, the flow field shows no substantial dynamics.

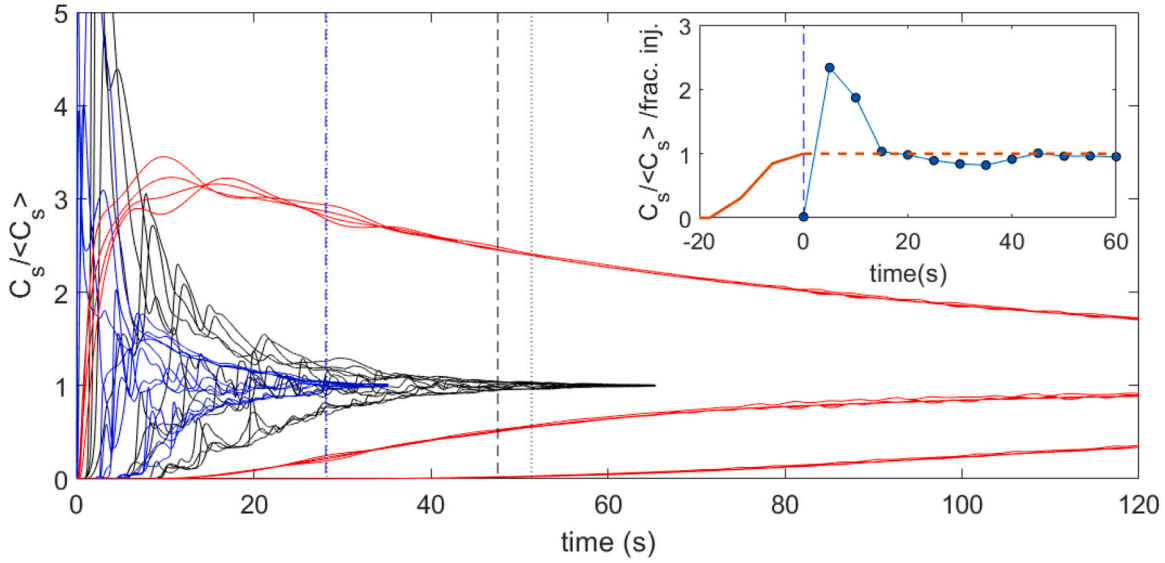

Fig. 5. Mixing curves for CFD Case B (blue), C (red) and D (black), registered at 12 locations in the reactor. The dashed vertical lines indicate the point-maximum 95 % mixing time, the dotted vertical lines the 95 % mixing time using the coefficient of variation. The expected mixing time based on Groen et al. is 46.0 – 56.7 s. Inset: experimental mixing data for $M_{liq} = 1,500kg$, $Q_g = 1,000\, l/\text{min}$. Orange line: MgSO4 injection curve (normalized). Blue dots: ICP measurements of Mg (liquid sampled from bottom).

Table 5
mixing time registered with CFD simulations for Cases B, C and D. Col 2: registration by probe with the longest mixing time. Column 3: registration as the CoV over all 12 probes, with a threshold of 0.0283 [65]. Column 4: 95 % mixing time estimated by the correlation of Groen [72].

Case	τ_{mix} ('worst' probe)	τ_{mix} (CoV)	τ_{mix} (Groen est.)
B	28.1 s	28.3 s	46.0 ($H_0 = 4.6$ m)
C	> 250 s	> 250 s	46.0 ($H_0 = 4.6$ m)
D	47.6 s	51.4 s	56.7 ($H_0 = 5.1$ m)

Unfortunately, no experimental mixing data was collected for the conditions under investigation. Experimental data is available for [1500 kg, 1000 L/min, 15 psi], by addition of $MgSO_4$ to the reactor top, and quantification of the Mg concentration through ICP of offline samples acquired at $h_{sample} = 0.23m$ every 5 seconds. The registered tracer response curve is shown in Fig. 5, inset. We note that both the long tracer injection duration and the analysis based on offline sampling complicate analysis; as such, the experimental values should be considered a ballpark estimation. With homogeneity observed 45 s after injection and an 18 s injection time (Fig. 5, inset, orange line), the ballpark mixing time is 45 – 58 seconds. This value is consistent with Groen's mixing

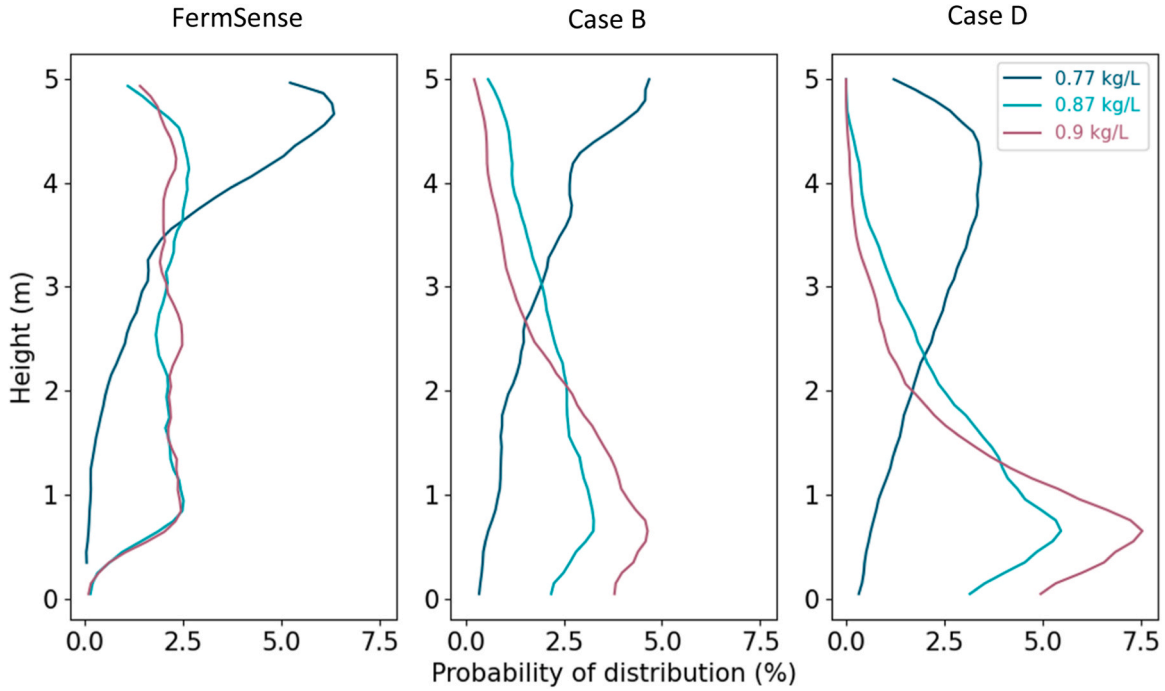

Fig. 6. Probability distributions of observing the sensor devices at a particular axial position (left) based on the cumulative local residence time vs. total experimental duration, versus the distribution in CFD Case B (middle) and D (right).

correlation, which yields $\tau_{mix} = 40.7s$, provided the flow is heterogeneous. Despite the low superficial gas velocity $\left(v_s = 0.017\frac{m}{s}\right)$, it is not unlikely that this is the case due to the coarse, non-ideal sparger being used in the current geometry [27,47]. Although the experimental mixing study was conducted at different operating conditions, this does indicate that mixing is in line with expectations based on the Groen correlation. Based on both the observations regarding the flowfield, and the strong disagreement between the computed mixing time and correlation, Case C considered unrealistic and not analyzed further in this study; Cases B and D are considered for further evaluation.

3.4. CFD results compared to sensor data

3.4.1. Device distribution

Fig. 6 shows the probability of presence of the FermSense sensors at different liquid height compared to the simulation results from Cases B and D; Cases A and C were discarded based on the grounds outlined above. Experimentally, the lightest sensor devices predominantly reside in the upper part of the liquid, which indicates flotation due to their density being substantially lower than that of the gas-liquid mixture [20], while the other two devices show an approximately uniform axial distribution in most of the column; the sensors are hardly observed below the sparger (0.23 m from the bottom). In the region just above the sparger the probability of observation is also lower, likely due to the strong upward velocity of gas emitted from the sparger holes, and the higher mixture density due to a lack of bubbles in surrounding liquid. The lightest device behaves qualitatively similar in the CFD simulations, but both heavier devices are more prone to settling than experimentally observed in both CFD simulations. The device of 0.87 kg/L has a density close to the apparent fluid density of Case B, yet we still observe settling behavior. The 0.9 kg/L particles show much more pronounced settling, in contrast to experimental observations. Despite an only moderately higher gas holdup, both the 0.87 and 0.9 kg/L particles show strong settling behavior, although the experimental finding that the probability of observation reduces in the bottom 0.5 m is consistently seen. Overall, it appears the Lagrangian particles in the CFD simulation are much more sensitive to (local) conditions than experimental devices. A potential explanation for the stronger settling behavior in the CFD simulations is that the particles are highly sensitive to the axial gradient in gas holdup owing to the hydrostatic pressure gradient [15], and are unlikely to reside in the vessel top where the apparent density is below the particle density.

This is markedly different for the experimental devices, where the similar behavior of the 0.87 kg/L and

0.9 kg/L devices supports a relatively low sensitivity to local and even global mixture density, which is supported by other studies at high gas velocity [19], although based on low gas velocity data some upward shift in the probability distribution would be expected for the lighter sensor [20], which we did not observe here. Probably this is due to the more vigorous fluid motions currently under consideration. Furthermore, we note that the aforementioned discrepancy between the laser level measurement and device density appears to support *reduced* rather than enhanced settling behavior, which contrasts our observations in the CFD simulations. Overall, there is a clear discrepancy between the experimental- and modelled behavior of devices, which is not just due to an offset in gas holdup, but evidence of shortcomings in the models used to simulate device motion.

3.5. Circulation time

Fig. 7 shows the profile of the circulation times for FermSense sensors and simulated representative particles for Cases B and D. Both the experimental and computational distributions are calculated based consecutive passages through four horizontal planes, distributed through the liquid height, with the first plane at 1 m height from the bottom of the liquid and a clearance distance of 1 m between the rest [11]. The circulation time for 0.87 kg/L and 0.9 kg/L sensor devices was similar, although the heavier devices exhibit a slightly more pronounced tail. To quantify the circulation behavior, we fitted a log-normal distribution based on the first 100 s of each distribution using python, to reduce the impact of the long and poorly quantified tail; the distribution is parameterized with the shape σ, scale $\exp(\mu)$, and location (peak shift), described in Table 6. The mean circulation time and standard deviation are calculated based on the properties of the log-normal

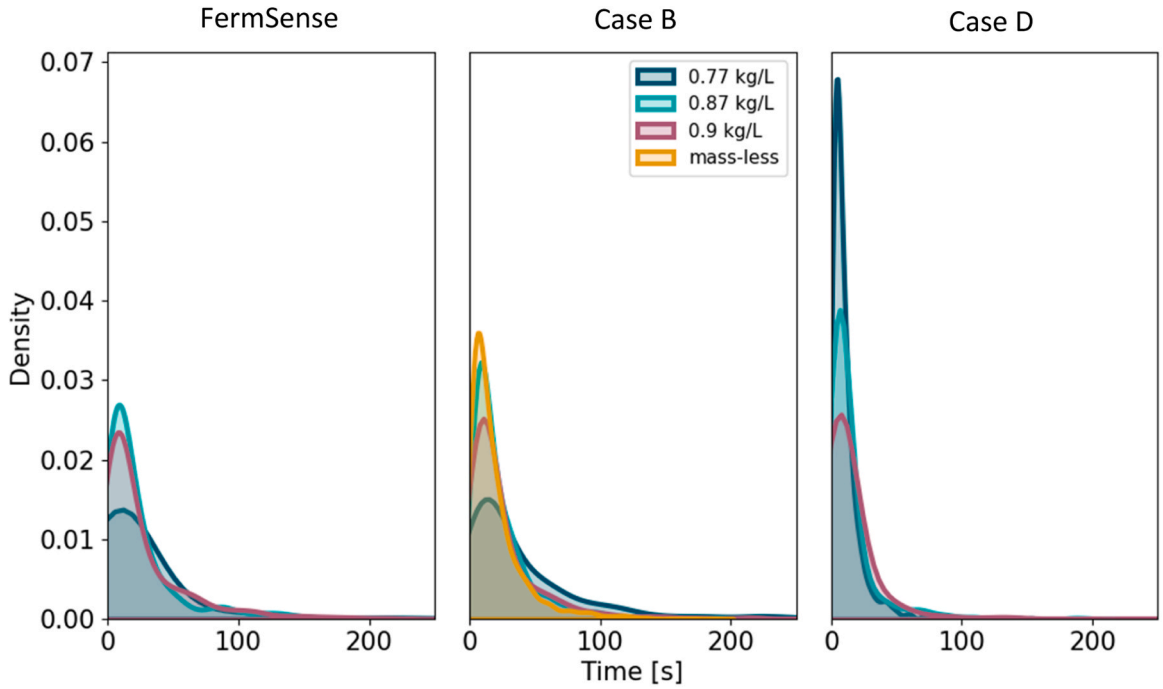

Fig. 7. Circulation times of the Freesense sensors and the CFD simulated particles based on the circulation plane methodology of Bisgaard et al. For Case B, trajectories of massless particles are shown for reference.

Table 6
Characteristics of the distributions in Fig. 7, estimated assuming a log-normal distribution in circulation behavior. Columns 3–5 provide the characteristics of the fitted log-normal object in python (scipy 1.10.1), estimated from the first 100 s of each distribution. Column 6, 7 provide the mean circulation time and standard deviation based on the log-normal distribution. Column 8 provides an alternative estimate of the circulation timescale based on fitting an exponential distribution to the downward slope of the circulation peak.

		log-normal distribution parameters					*Exp. decay*
Case	**Sensor**	**Shape**	**Scale**	**Location**	**Mean (s)**	**St. dev (s)**	τ_{circ} **(s)**
Exp.	0.77 kg/L	0.60	32	−7.1	38	25	23
Exp.	0.87 kg/L	0.85	17	−1.2	24	25	18
Exp.	0.90 kg/L	0.84	20	−1.4	28	29	19
CFD - B	0.77 kg/L	0.62	34	−7.5	41	28	34
CFD - B	0.87 kg/L	0.79	18	−1.4	25	23	17
CFD - B	0.90 kg/L	0.77	20	−2.0	27	25	17
CFD - D	0.77 kg/L	0.91	8	0.2	12	14	8
CFD - D	0.87 kg/L	0.88	12	−0.4	18	19	10
CFD - D	0.90 kg/L	0.73	16	−2.0	21	18	14

distribution and also reported in Table 6. The mean circulation times are in the order of 25 – 30 s, which may seem at odds with the rule of thumb $\tau_{mix} \approx 4\ \tau_{circ}$, based on the mixing time estimated using the Groen et al. correlation. This is in line with prior work by Bisgaard et al., who reported a proportionality constant of 2.2 and 2.6 for two different stirred tank configurations [11]. Reinecke et al. report a similar, albeit lesser, offset between particle-based and tracer-based circulation time [17]. An alternative circulation timescale can be estimated by fitting the downward slope of the main peak with an exponential distribution, $\exp(-\frac{t}{\tau})$. With this approach we observe typical values between 15 and 20 s for the well-circulating devices experimentally and in Case B, and around 910– 14 s in Case D. These values are reasonably in line. The experimental circulation time of the 0.87 and 0.9 kg/L sensor matches well with Case B for both approximations, while Case D shows more rapid circulation behavior. This is likely due to the more biased movement of the particles at either top or bottom of the liquid, which results in a high frequency of short circulation times at the corresponding circulation planes. Interestingly, the observations made with the Lagrangian model disagree with the Eulerian mixing study (Section 3.3.2), wherein Case D the mixing time was in agreement with prior mixing correlations, while mixing in Case B was unexpectedly fast. This is likely affected by the positional bias leading to shorter circulations times in Case D, however; a more homogeneous sensor distribution is required to allow for comparison between Eulerian and Lagrangian mixing.

3.5.1. *Velocity profile*

Fig. 8 compares the absolute axial velocity profile of the FermSense devices with that of particles in the CFD simulations. Both for the CFD and experimental data, the domain was divided in 100 axial compartments, where the average absolute axial velocity is determined over all velocity registrations (up- and downward) within the compartment.

Similar to the earlier analysis, the recorded axial velocity by 0.87 kg/L and 0.90 kg/L sensors show a similar profile through the liquid height. In comparison, the measured velocities by the lightest device also showed a comparable profile, particularly in the liquid height above 1.5 m. These results show the low sensitivity of the sensors' velocity to their adjusted density within the specified range. All three devices showed a slightly higher axial velocity at vertical center of the column, while the velocity goes down at the top and the bottom of the liquid.

In comparison to the experimental data, both CFD models predicted a slightly lower absolute velocity, with Case B being slightly closer to the experiments than Case D. The deviation between the data and the simulation results by both models increases at the higher liquid levels which can be due to the difference between the estimated gas holdup at

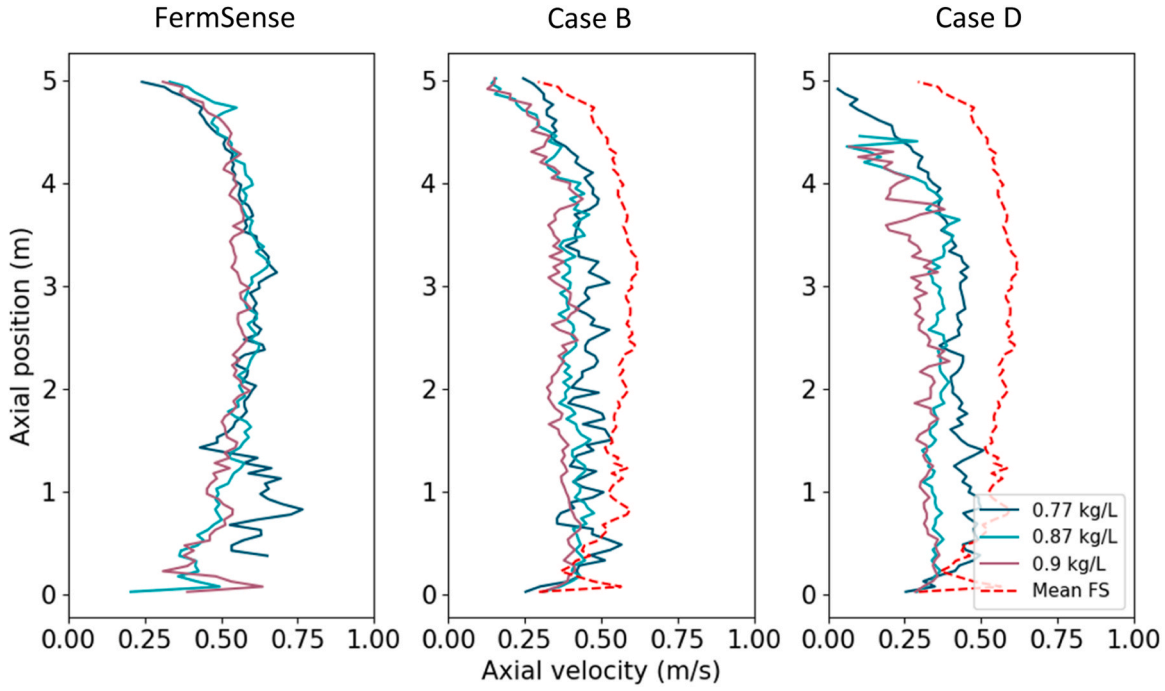

Fig. 8. Averaged absolute axial velocity of the Freesense sensors and the simulated particles, acquired by dividing the column in 100 axial compartments. The dashed red line in the middle- and right figures shows the experimental data (average of all devices) for reference.

the higher axial part of the liquid.

We can further compare the velocity profiles by looking at the local axial velocity distribution. Fig. 9 gives an overview of the distribution of the upward and downward velocities of the FermSense sensors compared to the simulated particles at different liquid height. The collected data from the FermSense sensor with density of 0.87 kg/L shows a profile within the range of ± 1.67 m/s, with most values registered in the range of ± 0.51 m/s (indicated by the yellow band) and uniformly along the liquid height. Although the overall range of registered velocity values is similar, the CFD models show a more narrow velocity distribution for the Lagrangian particles with a density of 0.87 kg/L (Fig. 9b, c), as indicated by the narrower yellow bands. As discussed before, both simulations predicted the dominant movement of 0.87 kg/L particles at the bottom part of the liquid.

3.6. Discussion

The high Stokes number of *FermSense* devices indicates that, even when neutrally buoyant, they will not be ideal flow followers; something that already leads to some offset in device- and fluid behavior in single phase flows [11,12]. In addition, the non-homogeneous gas distribution in high gas velocity bubble columns will induce further offsets between device- and mixture behavior. In spite of this, both the devices with 0.9 and 0.87 kg/L densities exhibited good and highly similar circulation under heterogeneous gas flow conditions, while the lighter device (0.77 kg/L) showed predominantly floating behavior. At first glance, these observations support a gas holdup in line with the Heijnen and van 't Riet correlation [27] (~13 %), rather than the Maximiano Raimundo et al. correlation [14] (~21 %). Interestingly, however, the level sensor indicated a hold-up of 20.5 %. Furthermore, the observation that both the 0.9 and 0.87 kg/L circulated equally well contrast with the findings of Reinecke et al., who did note a shift in probability distribution of observation for a 2 % offset in device density [20], albeit in a stirred, single-phase environment. Both observations can be qualitatively understood when considering prior work on flow-following sensors using radio pills by van Barneveld et al. [66], who determined the settling velocity of a 3 cm diameter device, density matched to water, at various gas hold-ups and observed a reduced settling velocity. For their device, the measured settling velocity was nearly constant for a 15–20 % gas holdup, and was equal to that expected in a 10 % holdup mixture. While different in details (sensor diameter, density), qualitatively these finding support both the magnitude of the observed effect, and the notion that the circulation behavior seems to only mildly sensitive to device density. Exactly why this reduction in settling velocity occurs is poorly investigated. We explored the hypothesis that radial gradients in gas hold-up play a role, and while indeed our terminal velocity model revealed some impact, the magnitude was insufficient to describe the gap fully. Still, this was a static model based on the average gradient, applied to a system that is highly dynamic in reality. One could, for example, hypothesize that sensor devices preferentially reside is regions of lower gas holdup, where friction is relatively higher. This would translate into a higher mixture density around the sensor (on average), and also increase the global gas holdup at which the sensor *acts* as neutrally buoyant. However, this effect would expect this effect to reduce upon increasing gas holdup, which contradicts the observations by van Barneveld et al. Other possible mechanisms are slipping of bubbles past the sensor, which could similarly increase the effective mixture density to which devices respond, or the adherence of bubbles to the device surface increasing buoyancy, as suggested by van Barneveld et al. [66]. A rough estimation shows a ~10 % reduction in effective density at ~20 % gas holdup is required for the observed reduction in settling velocity, which would require 50 % of the surface to be covered with a 1 mm layer of air. All in all, further investigation into the behavior of flow-following devices in aerated systems is required. A comparison against other experimental techniques is desirable. Ideally, optical tracking of devices in vigorous heterogeneous gas flow would be conducted. This may be challenging in 3D systems due to high holdups leading to opacity, but may be feasible in a 2D column. Naturally, when interpreting and using this data in model development, the restrictions of a 2D environment need to be carefully considered. Alternatively, we recommend a comparison between floating devices and other Lagrangian techniques such as radioactive particle tracking (RPT), as these are not hampered by opacity of the fluid. It does have to be considered that millimeter sized RPT-particles have much lower Stokes numbers, and since they are of similar dimension as gas bubbles, interact differently with the gas phase (i.e. preferentially reside in the liquid). As such they may require density matching with water instead of the mixture, and while they may give more representative data of the liquid flow inside the column, it may be challenging to compare their behavior with that of centimeter-scale devices.

The behavior of simulated sensors was analyzed in detail in two CFD simulations. In agreement with experimental data, the 0.77 kg/L sensors showed floatation behavior in both, although they were more likely to reach the lower column regions than in the experiments. The 0.87 and 0.9 kg/L particles were distributed throughout the column in both cases, but showed marked differences in the degree of distribution; both already exhibit some degree of settling in Case B, with a 12.6 % average holdup. This is clearly much lower than the experimental holdup according to the level sensor, and also conflicts with the experimental findings of van Barneveld et al. [66]: particles show somewhat *stronger* settling than expected based on the global holdup, and we do see a marked difference in settling behavior between the 0.87 and 0.9 kg/L

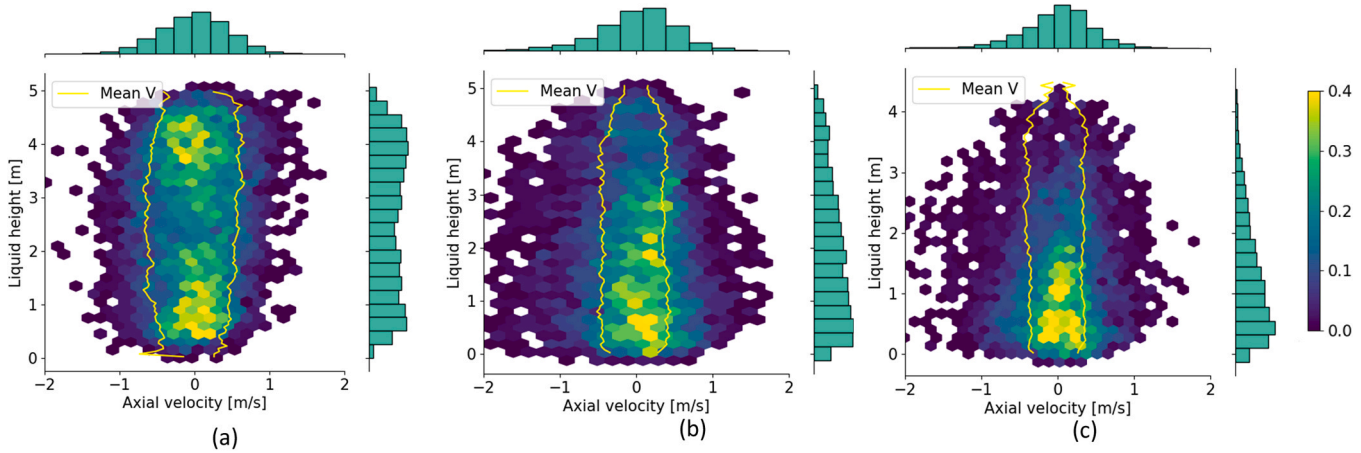

Fig. 9. Axial velocity distributions of the 0.87 kg/L device; a) experimental, b) CFD Cases B and c) CFD Case D.

particles which is consistent with their density difference, but not with experimental observations. If we zoom in further, the Fig. 6 reveals that the virtual particles are more prone to reside in regions with a mixture density equal to or higher than their own density; this is evidenced both by the 0.77 kg/L particles circulating deeper into the column than their experimental counterparts, and the heavier particles biased towards the column bottom, where, due to the axial holdup gradient resulting from gas expansion, the mean mixture density is somewhat higher.

These observations show that the current interphase interaction models applied to the particles are inadequate to describe the behavior of flow-following devices in a multiphase flow. The notion that very different settling behavior is observed between simulation and experiment suggests that indeed localized phenomena, such as very local low-holdup regions, bubbles slipping past the device to reduce effective holdup, or adherence of bubbles to reduce effective device density are at play – in contrast to large-scale holdup gradients and plume oscillations, these effects are not included in the CFD simulation. With more experimental insight in the behavior of flow-following devices in gas-liquid flow, it should be feasible to develop interaction models capturing such effects, e.g. a density correction based on local gas holdup. pressure gradient and virtual mass) should also be investigated separately to more insight in their contribution to the observed behavior. Of course, whether the other interphase interaction forces (drag, pressure gradient, virtual mass), which were developed for single phase fluid-particle flows, behave correctly in the current situation should also be subject to further investigation. Finally, we included the impact of turbulence through the dynamic random walk (DRW) model, which introduces a randomized velocity component to mimic the impact of turbulence on device behavior. Due to the substantial inertia resulting in a second-scale response time, this likely leads to excessive turbulent motion; a randomized force (instead of velocity) may lead to more realistic behavior, although perhaps the impact of turbulence could also simply be omitted. Overall, based on our current observations, the behavior of the experimental devices and simulated particles shows that the applied Lagrangian simulation approach currently does not accurately reflect real device behavior, and improvements in the gas-liquid-particle interaction model are needed if we want to use mobile sensor devices as a source of (circulation) validation data for CFD simulations. These results show that while theoretically mobile sensors can be used for CFD validation, but to do so, further insights are needed both in practical behavior of the sensors in (high-holdup) gas-liquid flows, and means of modelling this behavior.

Finally, we discuss some observations considering the Eulerian simulation results. We set out to simulate cases with high, moderate and low gas holdup. The gas holdup in the high-holdup Case (A) was excessive, leading to column overflow; the Richardson-Zaki swarm correction included in the universal drag model was clearly inadequate to capture the strong bubble drag reduction in a heterogeneous bubble column, in line with earlier observations [47]. In the first moderate holdup Case (C), we observed stable bubble plume formation, which was unexpected in light of prior studies [67]. The most notable difference is the exclusion Turbulent dispersion in our simulations due to stability issues, and other possible aspects (discretization schemes, mixture vs. dispersed turbulence, single bubble vs. population balance, McClure vs. Simonnet drag modification) were found to be non-influential. While the inclusion of turbulent dispersion seems to be essential when a holdup-based drag modification model is applied in this case, the general need for turbulent dispersion remains inconclusive, with some studies noting strong ‘flattening’ of holdup profiles compared to the parabolic profile observed practically [51]. However, these studies typically feature good initial bubble distribution due to a bottom-covering sparger, and do not include swarm modification models. Further study towards inclusion of turbulent dispersion is needed, both considering interaction with other interphase forces, and model stability. Considering the Eulerian mixing conducted in this work; we note that, due to the absence of bubble induced turbulence and consequent underestimation of energy dissipation in Case B, the rate of tracer mixing is over-estimated. This observation stresses that circulation behavior of high-Stokes inertial (Lagrangian) particles cannot be used to validate Eulerian mixing behavior – and that two simulations that are seemingly similar in terms of convective flow may differ substantially in terms of turbulent mixing if bubble induced turbulence remains unaccounted for.

4. Conclusion

We set out to study whether hydrodynamic data acquired with flow-following devices in heterogeneous bubbly flow can be used for validation of CFD models. In this respect, our results are ambiguous. The experimental work indicates that, despite high Stokes numbers and strong local variations in holdup, and hence apparent density, flow-following devices of reasonably matched density circulate through the entire column, and can provide relevant data for validation of (CFD) modelling studies. Because the devices are not perfect flow followers, the CFD simulations should include a Lagrangian (particle) phase to include non-ideal sensor behavior to facilitate comparison with experimental data. Our trials show we can successfully collect information on the circulation time, device velocity and distribution of devices among the axial coordinate from the timeseries of particle position, which provide a comprehensive dataset for validation; as the devices appear to act as neutrally buoyant over a range of at least several percents of gas holdup, the method is insufficiently sensitive to draw conclusions on overall gas holdup.

The approach to include the devices utilized in the current CFD study, with devices modeled as inertial point-like particles, does not seem to give an adequate representation of sensor behavior. A striking difference between experiment and simulation is that in practice the devices act neutrally buoyant at higher than expected global gas holdup, whilst in CFD simulations they do so at lower than expected global gas holdup. Part of the observed mismatch may be due to gradients in gas holdup, which means that global matching of the device and mixture density does not ensure local neutral buoyancy, but this does not explain why opposing trends are observed in practice and simulation. A second observation is that the particles in the CFD simulation are sensitive to small variations in (global) gas holdup, which does not align with the abovementioned observation that in practice, the devices act as neutrally buoyant over a range of at least several percents of gas holdup. Clearly, a better understanding of, and better models for the behavior of finite-size particles in gas-liquid flows is required, in particular in relation to their local environment, such as bubble adherence to sensors or the possibility that bubbles slip past sensor devices, affecting the effective density of the device and surrounding liquid, respectively.

Overall, the study indicates flow following devices have strong potential to provide insights in local bioreactor hydrodynamics and CFD validation, but that Lagrangian CFD models for the motion of sensor devices in gas-liquid require further study. We recommend studying the impact of the individual interphase forces acting on the particles as well – ideally with a resolved particle model - for deeper investigation with experimental data, and to study potential shortcomings of the inertial particle model. Such models additionally require much higher Eulerian resolution to properly resolve particle-fluid interaction, but with advances in GPU-based computing, this may be within reach [73,74]. In addition, further experimental scrutiny of the device behavior, e.g. in 2D columns allowing for optical comparison [75], or in comparison with radioactive particle tracking studies, would provide more insight in the observed offset with the static level sensor, as well as in the general behavior of high-stokes flow following devices is heterogeneous bubbly flow.

CRediT authorship contribution statement

Wouter A. van Winden: Writing – review & editing, Supervision,

Resources, Methodology, Conceptualization. **Tannaz Tajsoleiman:** Writing – original draft, Visualization, Validation, Methodology, Investigation, Formal analysis, Data curation, Conceptualization. **Cees Haringa:** Writing – original draft, Visualization, Validation, Software, Investigation, Formal analysis, Data curation, Conceptualization. **Ray M. Gladue:** Supervision, Project administration, Methodology, Investigation, Formal analysis. **Daniel Dong:** Writing – review & editing, Resources, Project administration, Methodology, Investigation, Formal analysis, Conceptualization. **Liang Wu:** Writing – review & editing, Supervision, Project administration, Methodology, Conceptualization. **Henk J. Noorman:** Writing – review & editing, Supervision, Methodology, Conceptualization. **Tue Rasmussen:** Writing – review & editing, Supervision, Resources, Project administration, Formal analysis, Conceptualization.

Declaration of Competing Interest

The authors declare the following financial interests/personal relationships which may be considered as potential competing interests: Authors WvW, LW, RG, DD and HN are full-time employees of dsm-firmenich AG. CH was an employee of dsm-firmenich AG at the time the original work was conducted. These authors have an interest in the end use of the technology. TT and TR are former employees of freesense ApS (now defunct), which had a commercial interest in the sensor devices. If there are other authors, they declare that they have no known competing financial interests or personal relationships that could have appeared to influence the work reported in this paper.

Data availability

The authors do not have permission to share data.

References

[1] H.J. Noorman, W. Van Winden, J.J. Heijnen, R.G.J.M. Van Der Lans, CHAPTER 1 intensified fermentation processes and equipment, RSC Green. Chem. 55 (2018) 1–41, https://doi.org/10.1039/9781788010320-00001. Vol. 2018-Janua.

[2] C. Haringa, et al., Computational fluid dynamics simulation of an industrial P. chrysogenum fermentation with a coupled 9-pool metabolic model: towards rational scale-down and design optimization, Chem. Eng. Sci. 175 (Jan. 2018) 12–24, https://doi.org/10.1016/j.ces.2017.09.020.

[3] D.D. McClure, H. Norris, J.M. Kavanagh, D.F. Fletcher, G.W. Barton, Towards a CFD model of bubble columns containing significant surfactant levels, Chem. Eng. Sci. 127 (May 2015) 189–201, https://doi.org/10.1016/j.ces.2015.01.025.

[4] R. Volger, L. Puiman, C. Haringa, Bubbles and broth: a review on the impact of broth composition on bubble column bioreactor hydrodynamics, Biochem. Eng. J. 201 (Jan. 2024) 109124, https://doi.org/10.1016/J.BEJ.2023.109124.

[5] O. Gunyol, H.J. Noorman, R.F. Mudde, CFD simulations of a large-scale fermenter with muliple impellers, Proc. 9th Int. Conf. Gas. Liq. Solid React. Eng. (2009) 1–4.

[6] C. Haringa, A.T. Deshmukh, R.F. Mudde, H.J. Noorman, Euler-Lagrange analysis towards representative down-scaling of a 22m3 aerobic S. cerevisiae fermentation, Chem. Eng. Sci. 170 (2017) 653–669, https://doi.org/10.1016/j.ces.2017.01.014.

[7] C. Bach, et al., Evaluation of mixing and mass transfer in a stirred pilot scale bioreactor utilizing CFD, Chem. Eng. Sci. 171 (Nov. 2017) 19–26, https://doi.org/10.1016/J.CES.2017.05.001.

[8] M. Kuschel, R. Takors, Simulated oxygen and glucose gradients as a prerequisite for predicting industrial scale performance a priori, Biotechnol. Bioeng. 117 (9) (Sep. 2020) 2760–2770, https://doi.org/10.1002/BIT.27457.

[9] C. Haringa, R.F. Mudde, H.J. Noorman, From industrial fermentor to CFD-guided downscaling: what have we learned, Biochem. Eng. J. 140 (Dec. 2018) 57–71, https://doi.org/10.1016/J.BEJ.2018.09.001.

[10] J. Bisgaard, et al., Flow-following sensor devices: a tool for bridging data and model predictions in large-scale fermentations, Comput. Struct. Biotechnol. J. 18 (Jan. 2020) 2908–2919, https://doi.org/10.1016/J.CSBJ.2020.10.004.

[11] J. Bisgaard, et al., Characterization of mixing performance in bioreactors using flow-following sensor devices, Chem. Eng. Res. Des. 174 (Oct. 2021) 471–485, https://doi.org/10.1016/J.CHERD.2021.08.008.

[12] S. Hofmann, C. Weiland, J. Fitschen, A. von Kameke, M. Hoffmann, M. Schlüter, Lagrangian sensors in a stirred tank reactor: comparing trajectories from 4D-Particle Tracking Velocimetry and Lattice-Boltzmann simulations, Chem. Eng. J. 449 (Dec. 2022) 137549, https://doi.org/10.1016/J.CEJ.2022.137549.

[13] C. Vial, E. Camarasa, S. Poncin, G. Wild, N. Midoux, J. Bouillard, Study of hydrodynamic behaviour in bubble columns and external loop airlift reactors through analysis of pressure fluctuations, Chem. Eng. Sci. 55 (15) (Aug. 2000) 2957–2973, https://doi.org/10.1016/S0009-2509(99)00551-5.

[14] P. Maximiano Raimundo, A. Cloupet, A. Cartellier, D. Beneventi, F. Augier, Hydrodynamics and scale-up of bubble columns in the heterogeneous regime: comparison of bubble size, gas holdup and liquid velocity measured in 4 bubble columns from 0.15 m to 3 m in diameter, Chem. Eng. Sci. 198 (Apr. 2019) 52–61, https://doi.org/10.1016/J.CES.2018.12.043.

[15] S.B. Kumar, D. Moslemian, M.P. Duduković, Gas-holdup measurements in bubble columns using computed tomography, AIChE J. 43 (6) (Jun. 1997) 1414–1425, https://doi.org/10.1002/aic.690430605.

[16] S. Hofmann, et al., Experimental analysis of lifelines in a 15,000 L bioreactor by means of lagrangian sensor particles, Chem. Eng. Res. Des. 205 (May 2024) 695–712, https://doi.org/10.1016/J.CHERD.2024.04.015.

[17] S.F. Reinecke, L. Buntkiel, R. Kipping, U. Hampel, Process characterization in industrial vessels by flow-following sensor particles, Meas. Sci. Technol. 33 (9) (Jun. 2022) 095106, https://doi.org/10.1088/1361-6501/AC75AF.

[18] C. Haringa, H.J. Noorman, R.F. Mudde, Lagrangian modeling of hydrodynamic–kinetic interactions in (bio)chemical reactors: practical implementation and setup guidelines, Chem. Eng. Sci. 157 (Jan. 2017) 159–168, https://doi.org/10.1016/j.ces.2016.07.031.

[19] J. Bisgaard, J.A. Zahn, T. Tajsoleiman, T. Rasmussen, J.K. Huusom, K.V. Gernaey, Data-based dynamic compartment model: modeling of E. coli fed-batch fermentation in a 600 m3 bubble column, J. Ind. Microbiol. Biotechnol. 49 (5) (Oct. 2022), https://doi.org/10.1093/JIMB/KUAC021.

[20] S.Felix Reinecke, U. Hampel, Instrumented flow-following sensor particles with magnetic position detection and buoyancy control, J. Sens. Sens. Syst. 5 (1) (Jun. 2016) 213–220, https://doi.org/10.5194/JSSS-5-213-2016.

[21] K.M. Davidson, S. Sushil, C.D. Eggleton, M.R. Marten, Using computational fluid dynamics software to estimate circulation time distributions in bioreactors, –6,, Biotechnol. Prog. 19 (5) (2003) 1480, https://doi.org/10.1021/bp025580d.

[22] T.P. Elson, D.J. Cheesman, A.W. Nienow, X-ray studies of cavern sizes and mixing performance with fluids possessing a yield stress, Chem. Eng. Sci. 41 (10) (Jan. 1986) 2555–2562, https://doi.org/10.1016/0009-2509(86)80041-0.

[23] J. van Barneveld, W. Smit, N.M.G. Oosterhuis, H.J. Pragt, Measuring the liquid circulation time in a large gas—liquid contactor by means of a radio pill. 2. circulation time distribution, Ind. Eng. Chem. Res. 26 (11) (Nov. 1987) 2192–2195, https://doi.org/10.1021/IE00071A004/ASSET/IE00071A004.FP.PNG_V03.

[24] S. Azizi, A. Yadav, Y.M. Lau, U. Hampel, S. Roy, M. Schubert, On the experimental investigation of gas-liquid flow in bubble columns using ultrafast X-ray tomography and radioactive particle tracking, Chem. Eng. Sci. 170 (Oct. 2017) 320–331, https://doi.org/10.1016/j.ces.2017.02.015.

[25] J. Chen, A. Kemoun, M.H. Al-Dahhan, M.P. Duduković, D.J. Lee, L.-S. Fan, Comparative hydrodynamics study in a bubble column using computer-automated radioactive particle tracking (CARPT)/computed tomography (CT) and particle image velocimetry (PIV), Chem. Eng. Sci. 54 (13–14) (Jul. 1999) 2199–2207, https://doi.org/10.1016/S0009-2509(98)00349-2.

[26] J.C. Middleton, "Measurement of circulation within large mixing vessels," *Resour. Energy*, vol. 2, pp. 15–36, 1979, Accessed: Sep. 15, 2024. [Online]. Available: https://scholar.google.com/scholar_lookup?title=Measurement of circulation within large mixing vessels&publication_year=1979&author=J.C. Middleton.

[27] J.J. Heijnen, K. Van't Riet, Mass transfer, mixing and heat transfer phenomena in low viscosity bubble column reactors, Chem. Eng. J. 28 (2) (Apr. 1984) B21–B42, https://doi.org/10.1016/0300-9467(84)85025-X.

[28] D.D. McClure, C. Wang, J.M. Kavanagh, D.F. Fletcher, G.W. Barton, Experimental investigation into the impact of sparger design on bubble columns at high superficial velocities, Chem. Eng. Res. Des. 106 (Feb. 2016) 205–213, https://doi.org/10.1016/j.cherd.2015.12.027.

[29] J. Chen, P. Gupta, S. Degaleesan, M.H. Al-Dahhan, M.P. Duduković, B. A. Toseland, Gas holdup distributions in large-diameter bubble columns measured by computed tomography, Flow. Meas. Instrum. 9 (2) (Jun. 1998) 91–101, https://doi.org/10.1016/S0955-5986(98)00010-7.

[30] J. Bisgaard, et al., Automated compartment model development based on data from flow-following sensor devices, Processes 9 (9) (2021), https://doi.org/10.3390/pr9091651.

[31] R. Rzehak, T. Ziegenhein, S. Kriebitzsch, E. Krepper, D. Lucas, Unified modeling of bubbly flows in pipes, bubble columns, and airlift columns, Chem. Eng. Sci. (2017), https://doi.org/10.1016/j.ces.2016.04.056.

[32] G. Besagni, F. Inzoli, T. Ziegenhein, D. Lucas, Computational fluid-dynamic modeling of the pseudo-homogeneous flow regime in large-scale bubble columns, Chem. Eng. Sci. 160 (Mar. 2017) 144–160, https://doi.org/10.1016/J.CES.2016.11.031.

[33] Z. Huang, D.D. McClure, G.W. Barton, D.F. Fletcher, J.M. Kavanagh, Assessment of the impact of bubble size modelling in CFD simulations of alternative bubble column configurations operating in the heterogeneous regime, Chem. Eng. Sci. 186 (Aug. 2018) 88–101, https://doi.org/10.1016/j.ces.2018.04.025.

[34] D.F. Fletcher, D.D. McClure, J.M. Kavanagh, G.W. Barton, CFD simulation of industrial bubble columns: numerical challenges and model validation successes, Appl. Math. Model. 44 (2017), https://doi.org/10.1016/j.apm.2016.08.033.

[35] E. Ertekin, J.M. Kavanagh, D.F. Fletcher, D.D. McClure, Validation studies to assist in the development of scale and system independent CFD models for industrial bubble columns, Chem. Eng. Res. Des. 171 (Jul. 2021) 1–12, https://doi.org/10.1016/J.CHERD.2021.04.023.

[36] J. Sanyal, S. Vásquez, S. Roy, M.P. Dudukovic, Numerical simulation of gas–liquid dynamics in cylindrical bubble column reactors, Chem. Eng. Sci. 54 (21) (Nov. 1999) 5071–5083, https://doi.org/10.1016/S0009-2509(99)00235-3.

[37] N. Varallo, G. Besagni, R. Mereu, Computational fluid dynamics simulation of the heterogeneous regime in a large-scale bubble column, Chem. Eng. Sci. 280 (Oct. 2023) 119090, https://doi.org/10.1016/J.CES.2023.119090.

[38] G. Yang, K. Guo, T. Wang, Numerical simulation of the bubble column at elevated pressure with a CFD-PBM coupled model, Chem. Eng. Sci. 170 (Oct. 2017) 251–262, https://doi.org/10.1016/J.CES.2017.01.013.
[39] M.V. Tabib, S.A. Roy, J.B. Joshi, CFD simulation of bubble column—an analysis of interphase forces and turbulence models, Chem. Eng. J. 139 (3) (Jun. 2008) 589–614, https://doi.org/10.1016/J.CEJ.2007.09.015.
[40] M. Pourtousi, J.N. Sahu, P. Ganesan, Effect of interfacial forces and turbulence models on predicting flow pattern inside the bubble column, Chem. Eng. Process. Process. Intensif. 75 (Jan. 2014) 38–47, https://doi.org/10.1016/J.CEP.2013.11.001.
[41] Z. Khan, V.H. Bhusare, J.B. Joshi, Comparison of turbulence models for bubble column reactors, Chem. Eng. Sci. 164 (Jun. 2017) 34–52. Accessed: Dec. 22, 2017. [Online]. Available: ⟨http://www.sciencedirect.com/science/article/pii/S0009250917300428?via%3Dihub⟩.
[42] I. Khan, M. Wang, Y. Zhang, W. Tian, G. Su, S. Qiu, Two-phase bubbly flow simulation using CFD method: a review of models for interfacial forces, Prog. Nucl. Energy 125 (Jul. 2020) 103360, https://doi.org/10.1016/J.PNUCENE.2020.103360.
[43] X. Yan, et al., Drag Coefficient Prediction of a Single Bubble Rising in Liquids, Ind. Eng. Chem. Res. 57 (15) (Apr. 2018) 5385–5393, https://doi.org/10.1021/acs.iecr.7b04743.
[44] D.A. Lote, V. Vinod, A.W. Patwardhan, Comparison of models for drag and non-drag forces for gas-liquid two-phase bubbly flow, Multiph. Sci. Technol. 30 (1) (2018) 31–76, https://doi.org/10.1615/MULTSCIENTECHN.2018025983.
[45] M. Simonnet, C. Gentric, E. Olmos, N. Midoux, Experimental determination of the drag coefficient in a swarm of bubbles, Chem. Eng. Sci. 62 (3) (Feb. 2007) 858–866, https://doi.org/10.1016/J.CES.2006.10.012.
[46] G. Yang, H. Zhang, J. Luo, T. Wang, Drag force of bubble swarms and numerical simulations of a bubble column with a CFD-PBM coupled model, Chem. Eng. Sci. 192 (Dec. 2018) 714–724, https://doi.org/10.1016/j.ces.2018.07.012.
[47] D.D. McClure, J.M. Kavanagh, D.F. Fletcher, G.W. Barton, Experimental investigation into the drag volume fraction correction term for gas-liquid bubbly flows, Chem. Eng. Sci. 170 (Oct. 2017) 91–97, https://doi.org/10.1016/J.CES.2016.12.066.
[48] D. Lucas, A. Tomiyama, On the role of the lateral lift force in poly-dispersed bubbly flows, Int. J. Multiph. Flow. 37 (9) (Nov. 2011) 1178–1190, https://doi.org/10.1016/J.IJMULTIPHASEFLOW.2011.05.009.
[49] D.D. McClure, J.M. Kavanagh, D.F. Fletcher, G.W. Barton, Development of a CFD model of bubble column bioreactors: part two - comparison of experimental data and CFD predictions, Chem. Eng. Technol. 37 (1) (Jan. 2014) 131–140, https://doi.org/10.1002/ceat.201300546.
[50] R.S. Oey, R.F. Mudde, H.E.A. van den Akker, Sensitivity study on interfacial closure laws in two-fluid bubbly flow simulations, AIChE J. 49 (7) (Jul. 2003) 1621–1636, https://doi.org/10.1002/aic.690490703.
[51] M.K. Silva, M.A. d'Ávila, M. Mori, Study of the interfacial forces and turbulence models in a bubble column, Comput. Chem. Eng. 44 (Sep. 2012) 34–44, https://doi.org/10.1016/J.COMPCHEMENG.2012.04.007.
[52] R.M.A. Masood, A. Delgado, Numerical investigation of the interphase forces and turbulence closure in 3D square bubble columns, Chem. Eng. Sci. 108 (Apr. 2014) 154–168, https://doi.org/10.1016/J.CES.2014.01.004.
[53] C. Laborde-Boutet, F. Larachi, N. Dromard, O. Delsart, D. Schweich, CFD simulation of bubble column flows: investigations on turbulence models in RANS approach, Chem. Eng. Sci. 64 (21) (Nov. 2009) 4399–4413, https://doi.org/10.1016/J.CES.2009.07.009.
[54] D. Zhang, N.G. Deen, J.A.M. Kuipers, Numerical simulation of the dynamic flow behavior in a bubble column: a study of closures for turbulence and interface forces, Chem. Eng. Sci. 61 (23) (Dec. 2006) 7593–7608, https://doi.org/10.1016/J.CES.2006.08.053.
[55] M.R. Rampure, S.M. Mahajani, V.V. Ranade, CFD simulation of bubble columns: modeling of nonuniform gas distribution at sparger, Ind. Eng. Chem. Res. 48 (17) (Sep. 2009) 8186–8192, https://doi.org/10.1021/ie8018593.
[56] Y. Wang, Q. Xiao, N. Yang, J. Li, In-depth exploration of the dual-bubble-size model for bubble columns, Ind. Eng. Chem. Res. 51 (4) (Feb. 2012) 2077–2083, https://doi.org/10.1021/ie200668f.
[57] R.M.A. Masood, A. Delgado, Numerical investigation of three-dimensional bubble column flows: a detached eddy simulation approach, Chem. Eng. Technol. 37 (10) (Oct. 2014) 1697–1704, https://doi.org/10.1002/ceat.201400173.
[58] P. Chen, J. Sanyal, M.P. Duduković, Numerical simulation of bubble columns flows: effect of different breakup and coalescence closures, Chem. Eng. Sci. 60 (4) (Feb. 2005) 1085–1101, https://doi.org/10.1016/J.CES.2004.09.070.
[59] F. Lehr, M. Millies, D. Mewes, Bubble-size distributions and flow fields in bubble columns, AIChE J. 48 (11) (Nov. 2002) 2426–2443, https://doi.org/10.1002/aic.690481103.
[60] M. Ishii, N. Zuber, Drag coefficient and relative velocity in bubbly, droplet or particulate flows, AIChE J. 25 (5) (Sep. 1979) 843–855, https://doi.org/10.1002/aic.690250513.
[61] A.A. Troshko, Y.A. Hassan, A two-equation turbulence model of turbulent bubbly flows, Int. J. Multiph. Flow. 27 (11) (Nov. 2001) 1965–2000, https://doi.org/10.1016/S0301-9322(01)00043-X.
[62] C. Haringa, et al., Euler-Lagrange computational fluid dynamics for (bio)reactor scale down: an analysis of organism lifelines, Eng. Life Sci. 16 (7) (Oct. 2016) 652–663, https://doi.org/10.1002/elsc.201600061.
[63] S.A. Morsi, A.J. Alexander, An investigation of particle trajectories in two-phase flow systems, J. Fluid Mech. 55 (2) (Sep. 1972) 193–208, https://doi.org/10.1017/S0022112072001806.
[64] A. Kukukova, J. Aubin, S.M. Kresta, A new definition of mixing and segregation: three dimensions of a key process variable, Chem. Eng. Res. Des. 87 (4) (2009) 633–647, https://doi.org/10.1016/j.cherd.2009.01.001.
[65] H. Hartmann, J.J. Derksen, H.E.A. van den Akker, Mixing times in a turbulent stirred tank by means of LES, AIChE J. 52 (11) (Nov. 2006) 3696–3706, https://doi.org/10.1002/aic.10997.
[66] J. van Barneveld, W. Smit, N.M.G. Oosterhuis, H.J. Pragt, Measuring the liquid circulation time in a large gas—liquid contactor by means of a radio pill. 1. Flow pattern and mean circulation time, Ind. Eng. Chem. Res. 26 (11) (Nov. 1987) 2185–2192, https://doi.org/10.1021/IE00071A003.
[67] W. Gu, E. Theau, A.W. Anderson, D.F. Fletcher, J.M. Kavanagh, D.D. McClure, A modelling workflow for quantification of photobioreactor performance, Chem. Eng. J. 477 (Dec. 2023) 147032, https://doi.org/10.1016/J.CEJ.2023.147032.
[68] J.A. Roels, J.J. Heijnen, Power dissipation and heat production in bubble columns: approach based on nonequilibrium thermodynamics, Biotechnol. Bioeng. 22 (11) (Nov. 1980) 2399–2404, https://doi.org/10.1002/bit.260221115.
[69] J. Gimbun, C.D. Rielly, Z.K. Nagy, Modelling of mass transfer in gas–liquid stirred tanks agitated by Rushton turbine and CD-6 impeller: a scale-up study, Chem. Eng. Res. Des. 87 (4) (2009) 437–451, https://doi.org/10.1016/j.cherd.2008.12.017.
[70] D.D. McClure, N. Aboudha, J.M. Kavanagh, D.F. Fletcher, G.W. Barton, Mixing in bubble column reactors: experimental study and CFD modeling, Chem. Eng. J. 264 (Mar. 2015) 291–301, https://doi.org/10.1016/j.cej.2014.11.090.
[71] R.G.J. van der Lans, K. van 't Riet, Mixing in bioreactor vessels," in Comprehensive Biotechnology, in: M. Moo-Young (Ed.), second ed.Engineering Fundamentals of Biotechnology, 2, Elsevier, Amsterdam, 2011, pp. 63–80.
[72] D.J. Groen. Macromixing in bioreactors, TU Delft, 1994.
[73] C. Haringa, An analysis of organism lifelines in an industrial bioreactor using Lattice-Boltzmann CFD, Eng. Life Sci. 23 (1) (Jan. 2023) e2100159, https://doi.org/10.1002/ELSC.202100159.
[74] J.A. Thomas, B. DeVincentis, N. Hanspal, R.O. Kehn, Predicting gas-liquid mass transfer rates in reactors using a bubble parcel model, Chem. Eng. Sci. 264 (Dec. 2022) 118183, https://doi.org/10.1016/J.CES.2022.118183.
[75] M.M. Mandalahalli, E.C. Wagner, L.M. Portela, R.F. Mudde, Electrolyte effects on recirculating dense bubbly flow: an experimental study using X-ray imaging, AIChE J. 66 (1) (Jan. 2020), https://doi.org/10.1002/aic.16696.